ABSTRACT

Title of Document: Upward Flame Spread Over Discrete Fuels

Colin H. Miller, Master of Science, 2014

Directed By: Dr. Michael J. Gollner, Assistant Professor,
Department of Fire Protection Engineering

Upward flame spread over discrete fuels has been analyzed through experimental research on vertical arrays of alternating lengths of PMMA and insulation. By manipulating the lengths of the PMMA fuel and the insulation, several important trends related to flame spread were identified and assessed.

The peak flame spread rate for arrays with 4 cm lengths of PMMA occurred at a fuel percentage of 67%; for arrays with 8 cm PMMA, a peak flame spread rate occurred at fuel percentages of 67%, 80%, and 89%. It has been hypothesized that increased air entrainment at these fuel percentages maximizes the flame spread rate.

Based on observed trends, this study proposed a method for approximation of the fuel spread rate at various fuel percentages. Given reasonable estimates for the homogeneous flame spread rate and the lowest fuel percentage that sustains spread, an estimation for intermediate spread rate values is feasible.

UPWARD FLAME SPREAD OVER DISCRETE FUELS

By

Colin H. Miller

Thesis submitted to the Faculty of the Graduate School of the
University of Maryland, College Park in partial fulfillment
Of the requirements for the degree of
Master of Science
2014

Advisory Committee:
Professor Michael J. Gollner, Committee Chair
Professor Stanislav I. Stoliarov
Mark A. Finney, PhD

Acknowledgements

First and above all, thanks and praise be to God. AMDG.

I want to thank the John L. Bryan Chair in Fire Protection Engineering for the funding to complete this thesis. I am truly blessed by the generosity of this fund, which enabled me to pursue an advanced degree that I otherwise would never have been able to afford. Over the past year, my passion for research has only grown, so I hope that this funding will prove to be the activation energy needed to incite a career where I can give back to the field of fire protection and the broader scientific community.

I would like to express my deep and sincere gratitude to Dr. Michael Gollner, who was involved in every step of this process. His willingness to work with me through all the difficulties of the experimental phase was incredible. The guidance I received from him was incredibly instrumental in pushing me towards the right direction and encouraging me during the low points. It was an honor and privilege to work under this man, whom I consider to be a true mentor.

I am also incredibly indebted to my fellow graduate students in the lab group: Daniel Gorham, Ajay Singh, Pietro Maisto, Zhao Zhao, and Brian Cohen. I'd particularly like to thank Daniel and Ajay for familiarizing me with the lab and for an unflagging willingness to assist with my experiments and side projects.

The help I received from undergraduate assistance was huge. These students, Stephen Ernst, Jonathan Kilpatrick, and Jeyson Ventura stuck with me through the many long hours spent cutting PMMA and welding thermocouples.

The Department of Fire Protection Engineering at the University of Maryland provided me with a great environment for the duration of my master's education. In addition to the amazing professors I've interacted with, I'd like to particularly thank Nicole Hollywood, Mary Lou Holt, and Sharon Hodgson for the assistance in managing details and deadlines that I could never have handled on my own.

A huge thanks to Dr. Christopher Cadou for the usage of the infrared camera. I am confident that I would not have been able to finish this project in time without the use of this technology, so I am truly grateful for this generosity.

Last, but certainly not least, I'd like to thank my family and friends for their continued support. I truly believe that the prayers of my parents have been instrumental in helping me throughout this process. Furthermore, the emotional support I received from my parents, all my siblings, and my friends was often exactly what I needed after many long hours spent in the lab.

Table of Contents

List of Figures

Chapter 1: Introduction

1.1 Motivation for Research

In 2012, at least 2,855 U.S. civilians lost their lives due to fire, U.S fire departments responded to 1.4 million fires, and an estimated $329 billion, or 2.1% of US GDP, was invested or lost in the fight against fire [1]. Given the magnitude of this "fire problem", further research within the field of fire protection engineering is essential to safeguarding our lives and investments as effectively as possible.

Flame spread, the process by which a flame moves across a flammable object, is an incredibly important phenomenon in fire scenarios. This phenomenon often governs the growth of a fire; in fact, it has been asserted that "in the initial stages of building fires, flame spread over the surface of combustible solid materials… is the key determinant of the rate of fire growth" [2]. In the interest of protecting lives and property from destruction due to fire, it must be of utmost importance to identify the underlying mechanisms related to flame spread. Moreover, upward flame spread over solids has been shown to significantly outpace both downward and lateral flame spread [3]. For this reason, upward flame spread is among the most important fire-based phenomena to address. Another important scenario where flame spread is very significant is in forced flow situations, where an externally-based wind accelerates flame spread in the streamwise direction. However, the research presented here will focus on experimental results from upward flame spread tests.

An investigation of the processes by which fire spreads across surfaces or between objects is vital to understanding the dangers of large-scale fires, such as those that can occur in a wildland fire or in a warehouse. Wildfire research has previously favored modeling focused on the radiant heat fluxes emitted by fires, but recent findings indicate that radiant heating will not ignite fine fuel elements under typical conditions [4]. Instead, convection and flame dynamics often govern this process, so smaller-scale flame spread analyses are relevant. Moreover, a typical fuel load in a wildland environment consists of many discrete, non-homogeneous fuels, which can be concentrated in varying densities. For this reason, it is important to understand the mechanisms by which fire spreads not only across a homogeneous surface but also between discrete fuels. Similarly, a warehouse typically features units of commodities which are stored in various discrete arrangements, covering up to 90% of the available floorspace [5]. In the event of a fire, flames can spread horizontally between commodities or vertically in the typical rack storage scenario. For this reason, it is important to understand expected phenomena of discrete fire spread, addressing whether discretization of fuels will accelerate, decelerate, or extinguish a spreading fire. An understanding of the associated geometry is essential to predicting fire behavior. The following study delves into an investigation of discrete fuels via empirical analysis of vertical flame spread.

1.2 Introduction to the Flame Spread Problem

Flame spread over solid fuels, at its most basic level, can be envisaged via a simple thermal model. Under normal circumstances, a typical solid fuel will remain at ambient temperature and

exhibit no combustion. However, if a sufficient influx of heat is introduced to a solid fuel, its temperature will rise and the fuel will undergo pyrolysis. Pyrolysis is a process whereby fuel undergoes a phase change to a gaseous state, thereby liberating flammable vapors from the solid. If enough flammable vapors are released by the material to form a flammable fuel-oxygen ratio, an ignition source (e.g., a spark, pilot light, or adjacent fire) can provide the threshold energy needed for combustion. If enough heat from combustion is reinvested into the solid fuel, a sustained reaction will occur whereby the solid continuously pyrolyzes and releases gaseous vapors. When this process is sustained, a flame will remain above the solid fuel.

The flame existing above this fuel reacts in a thin sheet known as a diffusion flame. This is the interface where fuel and oxidizer mix, resulting in a release of heat and combustion products. Typical combustion products of hydrocarbon fuels include carbon dioxide, water, carbon monoxide, soot, and other compounds. Approximate yields of combustion products vary depending upon the fuel being burned and the ambient conditions; additionally, the heat of combustion can vary for different fuels. Some fuels, such as wood, can form a layer of char that will remain behind after the rest of the material has burned. Other objects can melt, deform, or drip. The variability in behavior of fuels truly complicates quantification of flame spread, especially in the presence of soot, char, or deformations. Poly(methyl Methacrylate), or PMMA, is often chosen for flame spread research because it generally does not exhibit any of these confounding behaviors. Cast PMMA was chosen as the fuel of choice for this research project. Many studies have been conducted on flame spread over PMMA, and upward flame spread over PMMA has been fairly well documented [6-9].

Upward flame spread is much faster than downward or lateral flame spread because of the natural buoyancy of hot gases. This phenomenon allows the flame sheet and hot gases to naturally hover over a significant portion of the solid surface that has not yet been ignited. This flame sheet, in turn, heats the unburnt solid above the pyrolysis zone, so that it more readily reaches its ignition temperature and catches fire. A more detailed analysis of the thermal model associated with flame spread is discussed in the next section.

1.3 Flame Spread Models

As stated before, a simple thermal model is often employed in the analysis of upward flame spread. Several common parameters are important to understand in these models of flame spread. The first length scale to understand is the flame height, x_f, which simply refers to the height of the flame, from its base to its tip. Although a simple concept, the undulations associated with a realistic flame make measurement difficult, and no method of flame height calculation has been generally accepted by the research community as standard practice. Initially, experimentalists simply took the flame height by eying an appropriate value (occasionally from video footage) [10-13]. In 1995, Audouin et al. developed an image processing technique for pool fires where they averaged 160 images and obtained a flame presence probability [14]. The continuous flame height was then defined as the point where the presence probability was 95% and the maximum flame height as the height where presence probability was 5%. Gollner et al., Rangawala et al., and Consalvi et al. also used threshold values for video images to determine an appropriate flame height [15-17]. Consalvi et al. also linked the flame height to the heat flux

delivered to the fuel surface by means of a numerical model. A modified method of video image processing with a threshold value has been employed in this experiment, detailed in the experimental section. Despite variability in measurement techniques, the flame height is an important and recognized parameter in upward flame spread theory. Combustion occurs across the whole of the flame sheet, providing a heat flux that is both reinvested into the solid surface and released into the surrounding environment.

The whole of the flame height constitutes two major regions of interest at the fuel surface. The first region refers to the section of the fuel that is actually burning, and this is deemed the pyrolysis zone, x_p. The flame extension length, δ_f, also known as the pre-heating zone, constitutes the remainder of the flame height distance, and this is the region that is not currently burning but lies behind the impinging flame. In the pyrolysis zone, the fuel surface has reached its ignition temperature; consequently, the solid matter is pyrolyzing, leaving the surface as a hot gas, and eventually reacting with oxygen to form the diffusion flame. The diffusion flame extends over the flame extension length, providing a heat flux to this region of unburnt solid fuel. As this heat flux continues to heat the solid, more of the solid surface catches fire and the pyrolysis front marches upward. The rate of advancement of this pyrolysis front is, in fact, the flame spread rate. All of these length scales, x_f, x_p, and δ_f, will change with the transient effects of a vertically spreading flame. Many flame spread models take these length scales into account in the overarching thermal model, and these terms will be referred to in the remainder of this paper.

Figure 1.1 provides a graphical illustration of these length scales. If we define the bottom of the flame as $x = 0$, the pyrolysis region constitutes $0 < x < x_p$, the flame extension length $x_p < x < x_f$, and the flame height $0 < x < x_f$. The highlighted control volume in the flame extension

region is being supplied with a heat flux from the flame. In thermal models, a reasonable approximation of the magnitude and location of the heat flux is important because these parameters govern the rate at which the flame propagates. It is known that the heat flux in upward flame spread for many solids, including PMMA, decreases with height [18]. This experiment does not delve into examination of heat flux measurements, but it should be noted that a refined thermal model would likely benefit from a realistic heat flux approximation.

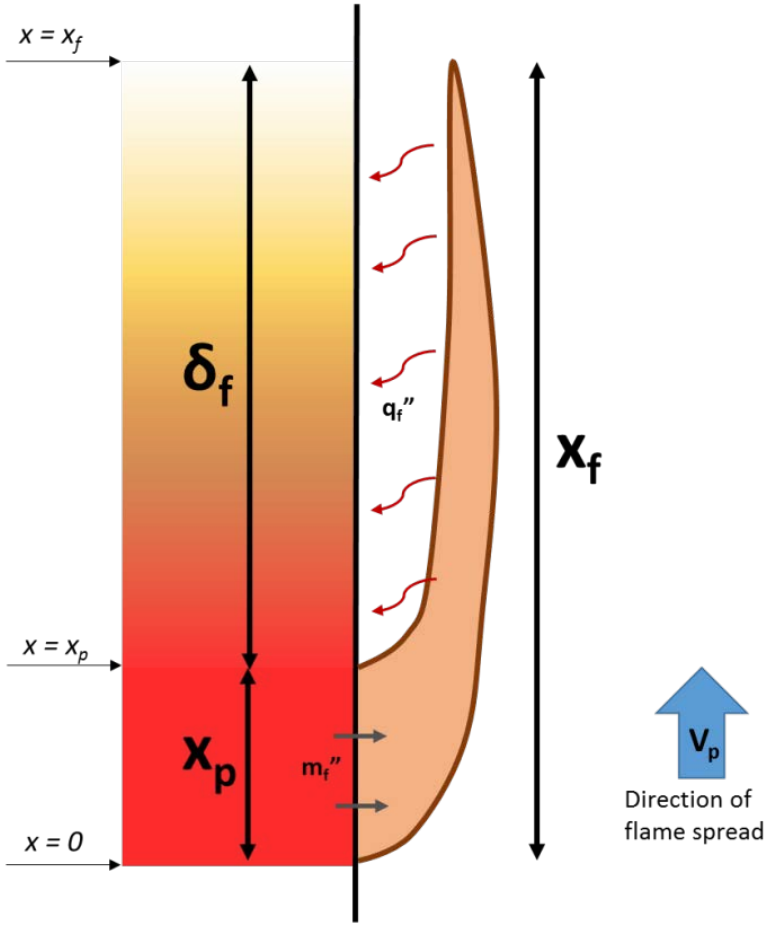

Figure 1.1. Illustration of important length scales and processes in a vertically spreading flame.

deRis presented the earliest theoretical solution for opposed flow spread, employing an energy balance to predict flame spread [19]. However, this model, in which conduction was the

primary mechanism of heat transfer, is not applicable to upward flame spread. In 1977, Williams was among the first to express flame spread as a simple thermal model via the "fundamental equation of fire spread",

$$V_p \rho \Delta h = \dot{q}" \tag{1.1}$$

where ρ is the density of the fuel, V_p the spread rate, Δh the difference in thermal enthalpy between the burning and unburnt fuel, and $\dot{q}"$ the heat flux applied to the unburnt fuel per unit area [20]. This equation is generally expanded into more familiar forms through assumptions for heat transfer processes. Williams supported the simplification of this fundamental equation by noting that the enthalpy change, in the absence of phase changes, can be written as $\Delta h = c_p(T_{ig} - T_0)$ where c_p is an average heat capacity per unit mass, T_0 is the initial temperature of the fuel, and T_{ig} is an ignition temperature. The concept of a constant ignition temperature is not always straightforward, as when measured via piloted ignition (for flame spread), it can vary based upon the measurement device and properties of the fuel, and may be less applicable to certain thermodynamically unique situations. Nevertheless, an ignition temperature has been demonstrated to be a valid criterion in most cases of flame spread and will be employed in subsequent discussions.

In analysis of flame spread, separate models exist for solids of different thermal thicknesses. A thermally thin solid is defined as thin enough such that heating effects in the form of a temperature gradient will be felt through the whole solid before the ignition temperature is reached. In a thermally thick solid, this thermal penetration depth will be less than the depth of the solid. Our study is centered on thermally thick solids, and, as such, a first order approximation of the flame spread rate can be expressed as

$$V_p = \frac{4(q_f")^2 \delta_f}{\pi(k\rho c_p)(T_{ig}-T_s)^2}, \quad (1.2)$$

where δ_f is the length over which the heat flux, $q_f"$, is applied, k is the thermal conductivity of the fuel, ρ the fuel density, c_p the specific heat, and T_s the initial fuel surface temperature [21]. Essentially, this approximation posits the flame spread rate as a ratio of the flame extension length to the time needed to bring the material to ignition. It considers only the most fundamental variables in flame spread and is often dependent on a proper selection of δ_f. This variable is often experimentally measured, and a reasonable estimation of the flame spread rate requires the selection of δ_f that is truly representative of the conditions. This variable is often derived from the flame length, which in turn is calculated from correlations available in the literature.

1.4 Inability of Models to Evaluate Discrete Fuels

In the following study, upward flame spread across discrete fuels will be studied. In our proposed experiment, the typical upward flame spread test is modified to introduce alternating vertical lengths of fuel and insulation. Most previous studies have focused on quantifying upward flame spread across continuous, homogeneous fuels, and this phenomenon is described by the aforementioned models. Introducing disconnected fuels into the scenario leads to a whole host of new questions. Appeals to previous theories can provide insight into these inquiries, but the variability associated with discrete fuels seems to imply that new correlations are hardly simple modifications.

One of the first issues associated with discrete fuels involves discontinuities along the pyrolysis zone. Typically, the pyrolysis zone is continuous and easily defined as the distance

over the burning material. However, in a discrete fuel configuration, it is now conceivable that the burning region will consist of multiple sections of disconnected fuels. For this reason, different regions of the pyrolysis zone must be defined. The "total pyrolysis zone", or $x_{p,total}$, refers to the distance associated with both the burning PMMA and the insulation that may lie between. The "fuel pyrolysis zone", $x_{p,fuel}$, is the total vertical distance of burning PMMA fuel; this distance represents the true pyrolysis region. Lastly, the "inert pyrolysis zone", $x_{p,inert}$, consists of the insulation that lies in between the burning PMMA. All three definitions would then be related by the following equation,

$$x_{p,total} = x_{p,fuel} + x_{p,inert}. \tag{1.3}$$

Figure 1.2 displays a side-view diagram of a vertical fuel array with alternating lengths of fuel and inert material. The total pyrolysis zone consists of three blocks of fuel contributing to the fire along with two sections of the inert wall. $x_{p,fuel}$, and $x_{p,inert}$ can be determined from our previous definitions, which lead to the following equations:

$$x_{p,fuel} = \sum_i x_{p,f(i)} = x_{p,f(1)} + x_{p,f(2)} + x_{p,f(3)} \tag{1.4}$$

$$x_{p,inert} = \sum_i x_{p,inert(i)} = x_{p,inert(1)} + x_{p,inert(2)} \tag{1.5}$$

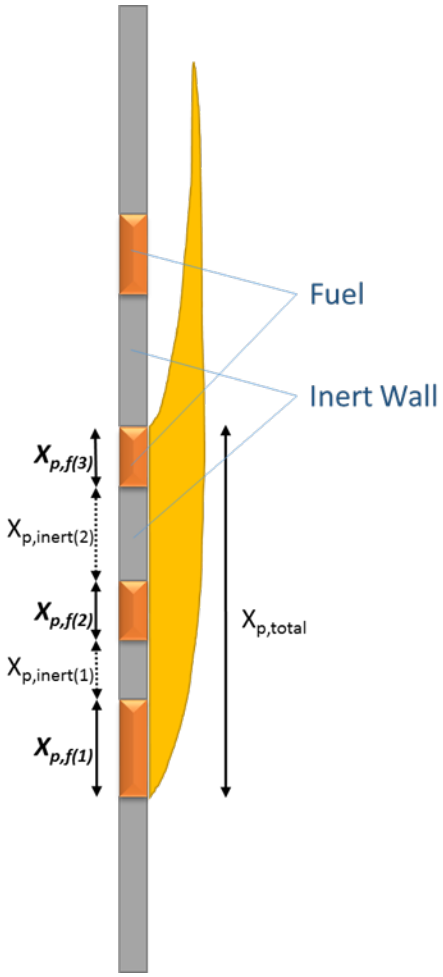

Figure 1.2. Graphical representation of a vertical array of discrete fuels.

It must be recognized that many previous correlations and models no longer apply to scenarios with discontinuous pyrolysis zones. Flame height correlations, which are often based on the length of the pyrolysis zone, will not be directly applicable to discrete fuel scenarios. In turn, flame height estimates are occasionally used to establish the flame extension length, so the processes for calculating δ_f, an important parameter for thermal models of flame spread, will have to be differentiated from existing models.

In the typical upward flame spread scenario, the burning area is computed as the product of the total pyrolysis region and the width of the burning material. In discrete flame spread, a more appropriate burning area, A_{burn} would be

$$A_{burn} = x_{p,fuel} * width. \tag{1.6}$$

This new burning area should be utilized to determine the mass flux of fuel from the surface via the common equation

$$\dot{m}'' = \frac{\dot{m}}{A_{burn}}. \tag{1.7}$$

The flame spread rate, V_p, is another parameter that must be clarified for discrete cases. This refers to the velocity at which the pyrolysis front travels across a surface. In discrete fuel configurations, it must be realized that the pyrolysis front will reach the edge of one unit of fuel and temporarily halt. If more fuel is oriented nearby, the flame will steadily raise the temperature of this adjacent unit until it also begins to pyrolyze and ignite; a new pyrolysis front will then spread across its surface. These discontinuities in the spread of the pyrolysis front complicate measurement of the spread rate, V_p. Throughout the remainder of this paper, the flame spread velocity (or flame spread rate), V_p will refer to the total vertical distance traversed by the pyrolysis front over time. This distance was previously defined as $x_{p,total}$, which includes both combustible and non-combustible regions. Defined this way, the flame spread rate continues to be the rate at which flame spreads across the fuel arrangement in the direction of interest. However, a quantification of the rate at which the pyrolysis front moves across the fuel is also relevant. This parameter is the fuel spread velocity (or fuel spread rate), $V_{p,fuel}$, and it refers to the distance *of fuel* traversed by the pyrolysis front over time. Unlike the flame spread velocity, calculation of

the fuel spread velocity excludes any non-combustible region. Under a homogeneous flame spread scenario, this velocity will necessarily be equal to the spread rate; however, $V_{p,fuel}$ will always be less than the spread rate for discrete fuels. The fuel spread velocity is an important parameter because it indicates how quickly a certain quantity of fuel is becoming involved in the flame spread process. A fast fuel spread velocity indicates that a significant amount of fuel is quickly contributing to the overall heat release rate of a fire. On the other hand, a fast flame spread velocity may or may not indicate that a large amount of fuel is burning because calculation of V_p includes inert regions for discrete scenarios. Distinction of these two parameters will be maintained in subsequent discussions.

It should also be noted that experimental techniques of this project examine flame spread only in the upward vertical direction. For this reason, the flame spread velocity and the fuel spread velocity are oriented in the upward vertical direction unless otherwise indicated.

1.5 Previous Research on Upward Flame Spread

The experimental approach taken in this study focuses on upward flame spread over PMMA. Significant experimental research has already been conducted on flame spread in the vertical direction over homogeneous sheets of PMMA. Vertical flame spread presents one of the most dangerous fire hazards because the natural buoyancy allows for concurrent flame propagation and accelerating flame spread [22]. Drysdale and MacMillan studied effects of fuel orientation on the flame spread rate, and found substantially higher velocities as the angle of orientation approached the vertical [23].

Average rates of upward flame spread over PMMA have also been quantified by various researchers. As a few examples of flame spread measurements over small samples of PMMA, Drysdale and MacMillan measured an average spread rate of 0.085 cm/s with sidewalls and a width of 6 cm; Gollner et al. measured a rate of 0.065 cm/s with no sidewalls and a width of 10 cm; Pizzo et al. measured an initial rate of approximately 0.07 and 0.075 cm/s with no sidewalls and widths of 10 and 20 cm., respectively [9, 23, 24]. The variation in these measurements can be explained by the presence or absence of sidewalls, some variations in the measurement technique, different formalities of PMMA, ambient conditions, geometry of apparatuses, and the varying widths and thicknesses of fuels. Both sidewalls and widths are important factors in quantifying flame spread, and research on the effects of these parameters has been well-documented in recent years.

Rangwala et al. and later Tsai and Wan performed upward flame spread experiments on PMMA slabs of varying widths [25, 26]. Rangawala et al. stated that lateral diffusion is significant for widths less than 20 cm without sidewalls; Tsai and Wan found that width effects are significant for samples narrower than 30 cm in the presence of sidewalls. In the absence of sidewalls, Pizzo et al. recently found that both flame height and spread rate for flames wider than 10 cm is independent of width [27]. It was confirmed that as the width increases, a smaller fraction of the fire will be influenced by edge effects, notably the lateral diffusion of air in the absence of sidewalls.

Sidewalls are often employed in order to preserve two-dimensional flow patterns in upward flame spread, and it has been shown that sidewalls increase the flame height [22]. Furthermore, recent work done by Tsai indicates that flame heights with sidewalls remain higher

for widths of up to at least 70 cm [28]. Tsai posits that the decrease in flame height in the absence of sidewalls is due to increased air entrainment, as demonstrated by Figure 1.3. As more air is entrained, combustion becomes more efficient and the generated pyrolyzate is quickly consumed as it travels upward. This results in a shorter, but more efficiently-mixed flame. Returning to Equation 1.2, it is clear that the flame spread rate is proportional to $\delta_f (q_f")^2$, indicating that a tall flame with a high heat flux would attain the highest rate. But would a shorter, more efficiently-mixed flame in the absence of sidewalls propagate faster than a taller, less efficient flame due to sidewalls? Tsai's research, which included measurement of heat flux profiles, sheds light on this question as a function of width. For widths of 10 and 20 cm, the flame spreads faster with sidewalls; indicating that the effect of the taller flame height was stronger than that of the decreased heat feedback. Widths of 30 and 50 cm had similar spread rates with and without sidewalls. Meanwhile, the 70-cm-wide flame was fastest without sidewalls. In this instance, Tsai posits that a higher radiative heat flux overcomes the effect of the shorter flame height.

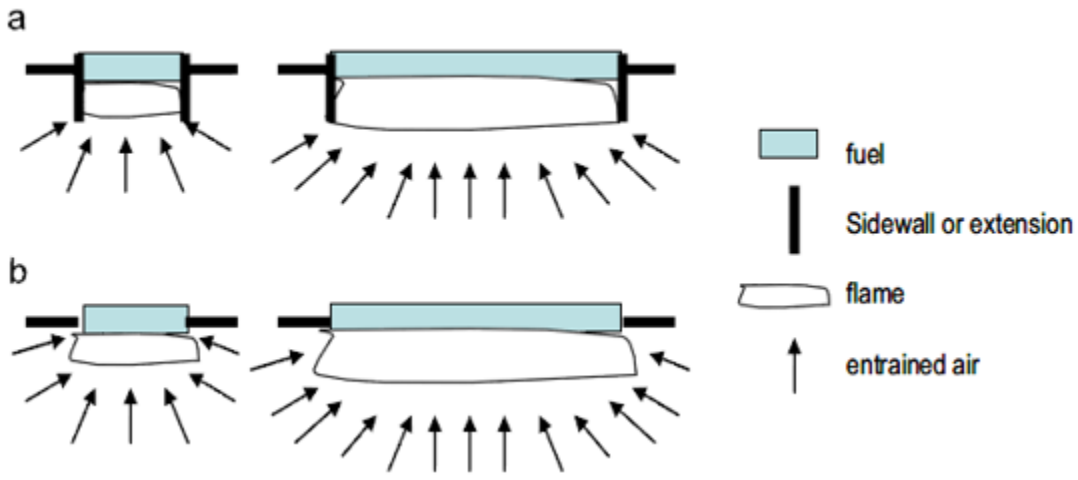

Figure 1.3. Schematic of different entrainment patterns of wall fires, reproduced from Tsai [28].

Given both the knowledge imparted by these previous studies and experimental constraints on width, the bulk of the work done in this study was performed on 20-cm-wide PMMA slabs with no sidewalls. Sidewalls, although designed to retain a 2-dimensional flow, are somewhat unrealistic [28]. Typical vertical fires do not spread in the presence of any sort of well-defined sidewall. Additionally, Pizzo demonstrated that, for flames of comparable proportion to those studied here, both flame height and spread rate were independent of width for flames wider than 10 cm [27].

It is also known that various geometric configurations can influence vertical flame spread properties. Tsai and Drysdale identified four such configurations, displayed in Figure 1.4, and analyzed the mass loss rates [29]. The configuration with an inner leading edge (case D) is the type of configuration tested in this project, and this setup produced the tallest flames. Unfortunately, Tsai and Drysdale did not record spread rates, but it is plausible to suppose that each configuration might lead to varying spread rates.

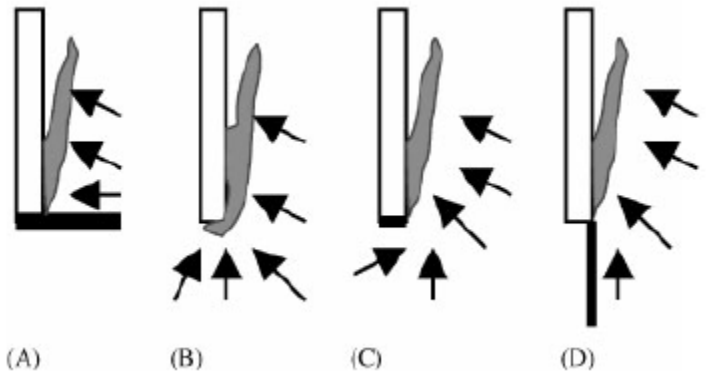

Figure 1.4. Schematic of four configurations which influence air entrainment of wall fires. Case D, which possesses an inner leading edge, is the configuration used in this study. Reproduced from Tsai and Drysdale [29].

It must be noted that vertical flame spread is not always steady. Upward flame spread over PMMA may begin at a steady pace, but experiments with samples of necessary height have observed significant acceleration of the flame spread rate [30]. The bulk of the subsequent analyses in this paper utilize averaged flame spread rates, but accelerative effects are examined and noted. In addition to the transient flame spread rate, the mass loss rate per unit area has been found to decrease as the pyrolysis zone advances [7, 28].

1.6 Previous Research Related to Homogeneous Discrete Fuels

Relatively few research projects on flame spread between discrete fuels have been undertaken. However, there have been a handful of papers published that document the results of similar experimental scenarios, most focusing on regimes where assumptions of a homogeneous fuel bed can be taken. For example, Thomas developed correlations for porous fuel beds of various materials, studying both natural convection and external forced flow scenarios [31, 32]. He determined that horizontal flame spread was inversely proportional to the bulk density of fuel for both scenarios. This means that, for the range of arrays that were studied, an increased density of fuel actually inhibited flame spread; indeed, this implies that the spread of the fire is most likely oxygen-limited. Meanwhile, flame spread was positively correlated with the external flow velocity, which could very well be a result of both a larger flame extension length and an increase in air entrainment. Subsequently, Dupuy performed experiments with

flame spread over various fuel beds and reaffirmed the trend for the flame spread rate to decrease with fuel density; however, he did not find Thomas's linear proportionality, instead invoking a power law of the form $R \sim {w_0}^b$ where R is the spread rate in mm/s and w_0 is the weight of the fuel bed per floor area in kg/m^2 [33]. After testing two pine needle fuel beds of varying densities, he found proportionalities where $b = 0.33$ and $b = 0.53$.

Rothermel formulated an excellent characterization of flame spread in porous fuel beds in his mathematical model for wildland fuels [34]. In addition to hypothesizing a slow rate of flame spread for densely packed fuels, he also theorized a decrease in the spread rate as fuel density decreased beyond a certain threshold. In the loose arrangement, a lack of fuel and heat losses would result in slower spread rates. Therefore, it was hypothesized that there would be an optimal fuel density for flame spread. Rothermel characterized this density within a "packing ratio" term. Experimental results confirmed this correlation, and this is reproduced in figure 1.5. It should be noted that the optimal packing ratio for flame spread rates varied based upon the type and size of the fuel.

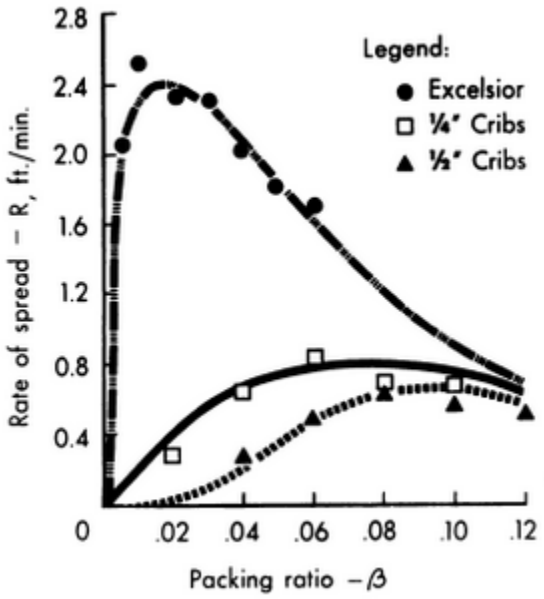

Figure 1.5. Relationship of the spread rate to the packing ratio. Note that an optimal spread rate occurs at intermediate values of the packing ratio. Reproduced from Rothermel [34].

1.7 Previous Research Related to Discrete Non-Homogeneous Fuels

Some research has also been conducted on discrete fuels in which an assumption of homogeneity is not readily appropriate. These experiments generally involve flame spread across discrete fuel elements as opposed to flame spread across a homogeneous material or fuel bed.

Studies on horizontal flame spread across discrete cellulosic fuels with varying properties have been performed. Emmons and Shen studied horizontal fire spread in arrays with paper strips standing on edge, while varying the height of the strips and the spacing between them [35]. Individual flames were observed from each piece of paper when the spacing was large, but these

flames would merge if the spacing became small enough. The spacing threshold beyond which merged flames would dissimilate was approximated as a linear function of paper height. Meanwhile, Finney et al. fabricated artificial fuel beds with horizontal discontinuities to look at thresholds in wildfire spread [36]. The length scales on these tests were quite large compared to most other discrete fuel tests, as an apparatus of 4 m in length and 1.2 m in width was employed. Vertical metal rods would sit on top of this apparatus, and these rods would be covered in excelsior at up to 120 cm in height. Flame spread between the gaps in the rows of fuel occurred due to flame contact; in some marginal spread cases, small firebrands caused flame spread. The contribution of non-steady flame contact in the spread of flames led Finney et al. to determine that a statistical interpretation was most suitable for this type of small-scale fire modeling. Their results suggest that the slope of the apparatus and the spacing between the fuels would contribute significantly to this statistical interpretation.

Two recent experiments have focused on the effects of porosity on flame spread across filter paper. These experiments have moved towards examination of discretized fuels by looking at the effects of both combustible and non-combustible regions. The first set of experimentalists, Watanabe et al., looked at flame spread across horizontal, combustible filter paper perforated with holes [37]. It was found that the flame would always spread across gaps of 4 mm or less but fail to spread across gaps of 8 mm or more. Watanabe et al. determined that this was an effect of the ratio of the pre-heating length δ_f to the pore length. When the pre-heat length exceeded the gap, the flame would spread; when the pore length exceeded the pre-heat length, no spread would be attained. For the two-dimensional array of perforated filter paper, a gap that spanned the entire apparatus (perpendicular to the direction of spread) was deemed a slit. The probability

for a flame to traverse a slit was closely related to whether the slit length exceeded the pre-heat length, with greater slit lengths resulting in low flame spread probabilities. The flame spread rate was also measured. An increase in the flame spread rate was observed as porosity increased from 0% to approximately 20 or 30%. Any further increase in porosity led to a decrease in the spread rate until approximately 50-60% porosity, at which point the flame failed to spread.

The aforementioned study took a less fundamental approach to discrete fuels by including randomization and lacking uniformity in both the spanwise and spreadwise dimensions. However, two important results should be recognized. First of all, it is clear that there is a threshold beyond which spread will not occur, and this threshold is directly related to the pre-heating length. Secondly, the data implies that the flame spread rate may reach a maximum velocity at a certain ratio of combustible to non-combustible material.

Abe et al. conducted experiments with an apparatus similar to Watanabe et al. [38]. They utilized filter paper with randomly distributed pores to simulate urban fires, which have regions of fuel (e.g., buildings) and areas that lack fuel (e.g., streets, empty lots). The filter paper was perforated with pores of 4 and 8 mm, and porosity levels of 40-60% were considered. The probability for the flame to spread across the filter paper was again determined to be very closely related to the number of slits formed, and the number of slits was positively correlated to porosity. The probability of successful flame spread across the apparatus was found to be close to 100% for 40% porosity (averaging almost no slits per test) and near to 0% for 60% porosity (averaging almost 2 slits per test).

Arrays of matchsticks (with the heads removed) have been utilized to study flame spread along discrete fuels. Several experimentalists have employed these arrays in studies of horizontal

flame spread. Vogel and Williams investigated flame spread between matchsticks in the horizontal direction, and they developed a theory including flame-standoff distance and ignition temperature which gave impressive agreement with experimental results [39]. Convective effects dominated heat transfer at these small scales. Prahl and Tien and Wolff et al. further investigated forced flow over horizontal configurations of matchsticks, Hwang and Zie looked at inclined matchstick spread, and Carrier et al. examined wind-aided flame spread across horizontal matchstick arrays [40-42].

Matchstick arrays are also useful mediums for investigating upward flame spread behavior. Recently, Gollner et al. examined discrete fuel behavior through an investigation of vertical matchstick arrays [43]. Flame spread over vertical arrays, or the "advancement of the ignition front", was found to be a function of spacing between the matchsticks. When the spacing was 0 cm, a linear fit was applied, but, as the spacing was increased to a maximum of 1.4 cm, power law dependencies were assumed due to buoyant acceleration. As the spacing between matchsticks was increased, the flame spread rate also increased. Even though the distance between fuel elements increased, the flame attained unobstructed impingement onto the next fuel element, resulting in faster spread. At some critical distance, however, the flame will fail to spread (although this distance was not investigated). Furthermore, in all setups where the spacing was greater than 0 cm, the pyrolysis front actually accelerated over the height of the array. Convective heat transfer correlations were found to nearly predict the burning behavior of this accelerating pyrolysis front.

It should be noted that nearly all previous experiments on flame spread over discrete fuels have been conducted with thermally thin fuels. Thermally thin fuels exhibit a minimal internal

thermal gradient, which can significantly alter the ignition process. In the following experiments, a new approach to flame spread research is taken, as only thermally thick fuels are employed.

1.8 Research Objectives

The primary objective of this study is to empirically analyze important parameters associated with upward flame spread over discrete fuels. The complexity of this problem should not be dismissed. Even the more fundamental case of upward flame spread over homogeneous fuel presents a transient problem. During the development of the fire, transient regions form within the flame itself; as a first-order approximation, these regions can be demarcated in terms of fluid mechanics properties (i.e., laminar vs. turbulent) or heat transfer mechanisms (e.g., radiant heat fractions). Much experimental work has been performed to identify these relevant mechanisms, which will vary widely depending on experimental conditions. In upward flame spread, the transient nature of these phenomena cannot be discarded because the flame front is changing as it moves vertically upward.

When this transient problem is coupled with a nonhomogeneous fuel surface, a whole host of new problems arise. Upward flame spread over discrete fuels will naturally involve a disconnected pyrolysis front, which changes the distribution of the mass flux released by the fuel. The flame itself will then be subject to different entrainment patterns, and it is possible for increased oxidizer to become available due to the gaps in the pyrolysis front. It is not fully known how the flame dynamics change in such a scenario: notably, it is not readily identifiable whether a disconnected pyrolysis front should be modeled as a single flame or multiple fires. Not only is

the pyrolysis zone disconnected, but also the unburnt fuel ahead of the flame front. The spacing of the fuel will influence which region of the flame has the greatest effect on the unburnt fuel; for example, significant spacing in a large fire may put the unburnt fuel in a zone where radiation effects become more important. If the spacing is beyond a certain threshold, extinction of the flame may also occur. In turn, the outcomes of all these scenarios are subject to the transient development of the flame front.

The significant number of unknowns associated with discrete fuels puts modeling of these parameters outside the realm of this study. Moreover, both physical limitations and time constraints limit the scales that can be tested. Nevertheless, this research project is a starting point in identifying expected trends for certain discrete fuel scenarios. By examining parameters that are necessarily intertwined with the flame spread, an understanding of expected discrete flame spread behaviors can be attained. Throughout this study, particular attention is focused on the relationship between the flame spread rate and the streamwise lengths of fuel and spacing. This relationship can elucidate the influence of factors relevant to flame spread over discretized fuels. Further correlations, including the mass loss rate and the flame height, are also studied. Results will further an understanding of discrete fuels, a common scenario for many real-world conflagrations.

Chapter 2: Experimental Work

2.1 Selection of PMMA as the Fuel of Choice

Several fuels were considered and tested before PMMA was selected as the optimal material for flame spread testing. Initial tests were conducted with thermally thin fuels, in an effort to find an easy and repeatable method for flame spread. The flame spread behavior of filter papers, paper towels, cardboard, and cheesecloth were all investigated in the laboratory; unfortunately, the results were disappointing. Uniform flame spread was nearly impossible to achieve when these thin fuels were held flush against an apparatus, horizontal or vertical. Various ignition sources were tested, including nichrome wire, liquid fuel wicks, blowtorches, and liquid fuel soaking. Regardless, flame spread consistently failed to spread uniformly, as areas of extinction often developed at irregular locations. There were a few occasions where flame spread over cheesecloth exhibited minimal extinction regions, but edge effects appeared significant across the whole breadth of a 20-cm-wide section of fuel. Several studies have found greater success by examining flame spread across suspended thin fuels, but the influence of air entrainment from both sides would not have allowed us to properly examine relevant discrete fuel behavior. Thin fuel flame spread also depends more heavily on the burnout region.

Thermally thick fuels were then considered for the experiment, and PMMA was selected as the fuel of choice. The entirety of this study is based on experimental results utilizing optically clear cast acrylic sheets of 1.27-cm-thick PMMA. As mentioned earlier, PMMA is a common choice for study because it has a simple degradation mechanism, and exhibits little to no soot,

charring, or deformations [44]. This material can also be cut and sized according to various experimental designs. The selected thickness of PMMA allowed for clean straight cuts with a band saw that would mount flush with 1.27-cm-thick Superwool 607 insulation boards. This thickness, furthermore, was enough to put the fuel into the thermally thick regime during the flame spread phase, meaning that the influence of the backing material is negligible in the relevant thermal fuel history in upward flame spread. Burnout of the PMMA was never observed for the duration of the tests although significant fuel recession was observed in the late stages of the tests, particularly at or just above the ignition source. For most successful flame spread tests, this recession appeared to occur after the entire apparatus had ignited and to have little influence on the actual spreading mechanism.

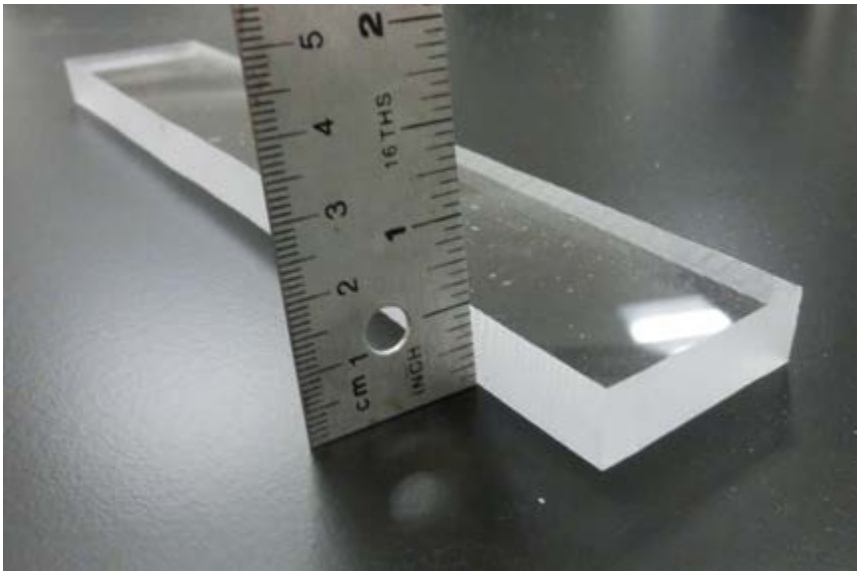

Figure 2.1. Photograph of PMMA sample (1.27-cm-thickness).

2.2 Test Apparatus and Experimental Design

The test apparatus needed for this experiment had to support discrete fuels in the proper vertical orientation while allowing for surface temperature measurements, video footage, and mass loss measurements. A 0.91-meter-tall apparatus was developed for this purpose, pictured in Figure 2.2. An aluminum frame was built to hold the apparatus in a 90° vertical position. A sheet of 91.5 x 48.5 cm plywood was bolted to the aluminum frame via brackets, and a sheet of 91.5 x 39.5 x 1.27 cm Superwool 607 insulation was held on top of this board. 91.5 x 2.5 cm aluminum shims were bolted on top of the insulation and ran the length of the apparatus vertically. These shims were used to hold alternating blocks of PMMA and insulation board against the apparatus. The shims provided a 20 cm exposure width for the PMMA and the insulation. The PMMA and the insulation were cut and sized for each experiment; both the PMMA fuel and insulation also were sized to a thicknesses of 1.27 cm, meaning that they could be held flush in the vertical direction by the shims. Unfortunately, the purchased insulation board was consistently about 1.5 mm thicker than the PMMA, meaning that there was always some variability in the flushness of the vertical surface between tests.

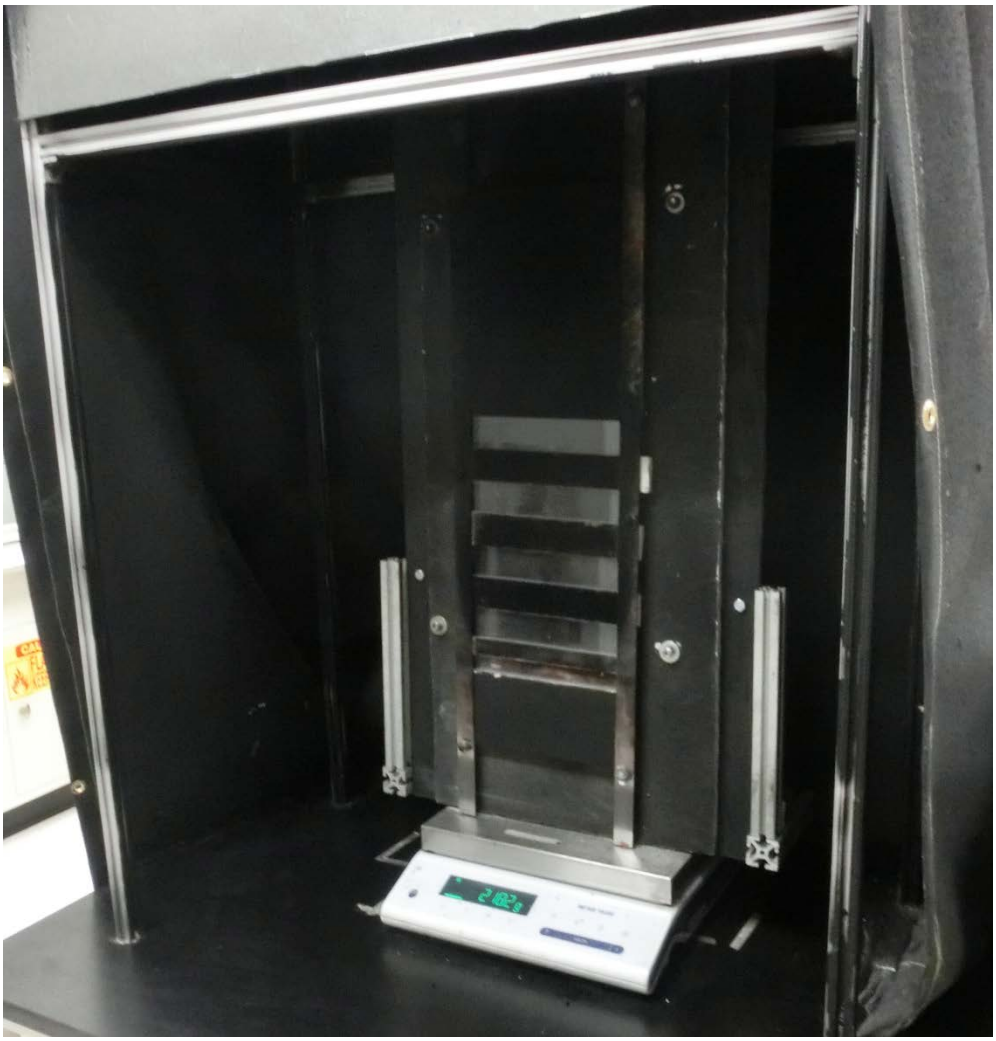

Figure 2.2. Photograph of apparatus to hold fuel array. The apparatus rested on a mass balance and was placed under an exhaust hood. The fuel array configuration displayed in this image contains 4 cm fuel and 4 cm insulation.

This entire contraption was then placed upon a mass balance so that the apparatus was held 12 cm above the surface of the table. This setup was safely positioned under a small exhaust hood and fitted with vertical, flameproof draperies on three sides, leaving the front section exposed. A Casio Exilim camera was positioned in front of this setup in order to record the flame height progression at 25 fps. A FLIR Thermacam SC3000 with a spectral response of 8 to 9 μm was also positioned in front of the setup; this camera operated using a 100-500°C filter with a user-

imposed image refresh rate of 4 fps. The only other notable physical components used in the experiment were the heat shield constituents, which were utilized during the ignition process. A small metal sheet and a larger, wood-based/metal-sheathed apparatus were employed to act as the heat shield. A thorough description of the heat shield's functionality can be found in the experimental procedure section.

2.3 Data Acquisition

Mass data was measured via the mass balance and sent to an adjacent computer. This mass data was recorded at 1 Hz on a balance that is sensitive to +/- 0.1 g, which allowed for reasonable accuracy. During the ignition process of each test, the measured mass would vary significantly due to the pressure being applied to the apparatus, but stabilization of these measurements occurred immediately after the removal of the ignition source and the heat shield.

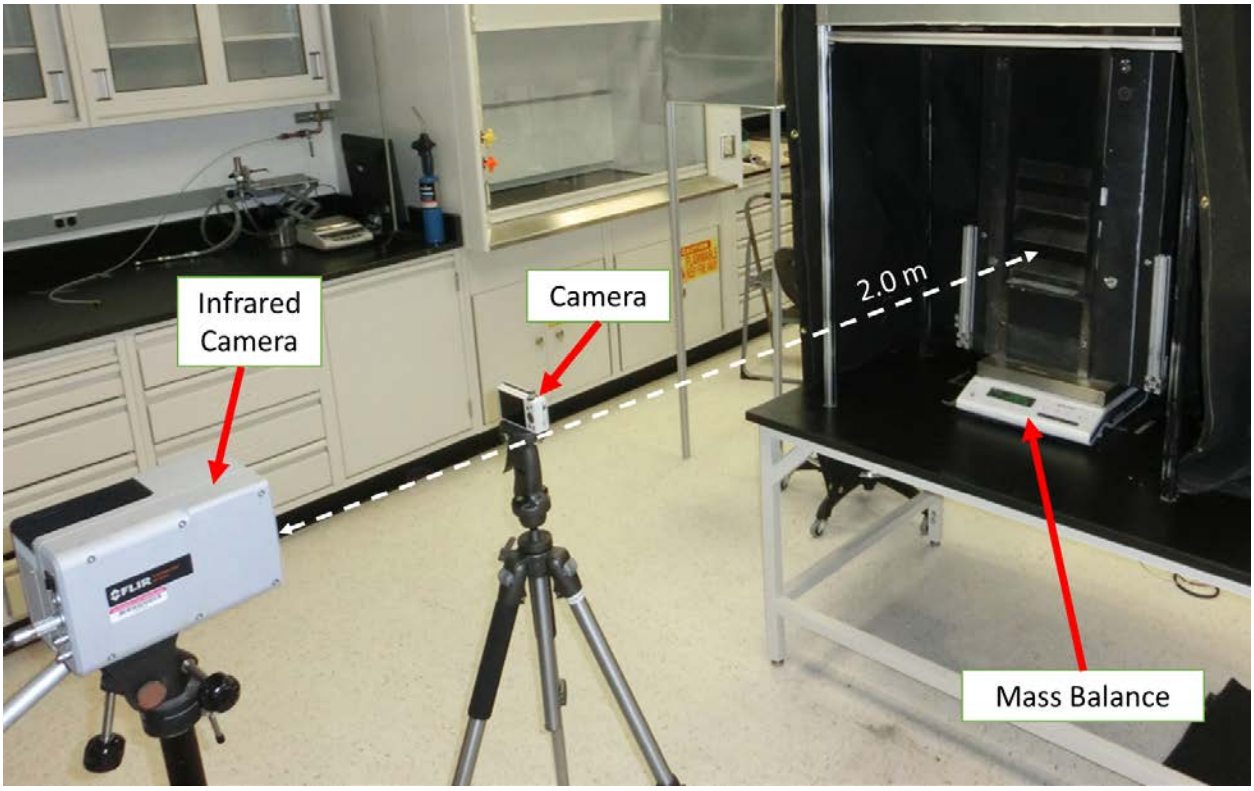

Figure 2.3. Photograph of apparatus and associated data acquisition equipment, including the mass balance, camera, and infrared camera.

The temperature of the PMMA was recorded via the infrared camera. The infrared camera was adjusted and focused to account for the viewing distance, which was typically 2 meters from the test apparatus. These temperature measurements were primarily meant to ascertain the location of the pyrolysis front. Determination of the location of the pyrolysis front by means of temperature measurement has been performed in various studies, and this process is based on the concept of an ignition temperature [30, 45, 46]. For the purposes of this study, the temperature at a certain height along the apparatus was calculated as the average temperature of a 2-cm horizontal centerline. Once the raw infrared temperature data was collected by an adjacent computer, it was analyzed by means of FLIR's Thermacam Researcher software. An emissivity of 0.92 was utilized in the images to ascertain the proper temperature of the PMMA; this value is

consistent with the emissivity utilized in transient experiments performed by Sohn et al. [47]. The reliability of the infrared images in determining the proper temperature of the PMMA was confirmed via tests with thermocouples, and it was determined that the infrared images were very closely correlated with the thermocouple measurements for an associated emissivity of 0.92.

Visual images throughout the test were simultaneously obtained through 25 fps camera footage. These images were saved onto the camera for post-processing of flame heights in MATLAB, a process that is described in section 2.7.

2.4 Establishment of a Discrete Fuel Array

The methodology of this research consists primarily in manipulating the vertical length scales within the fuel array. Consequently, the apparatus was designed to fit arrays with many different lengths of fuel and insulation. The bolts holding the aluminum shims to the body of the apparatus also served as base pegs to hold the first piece of insulation in the apparatus. These bolts would hold this first piece of insulation 10 cm above the bottom of the apparatus (22 cm above the table surface). The first piece of insulation was sized so as to establish a clear distance of upward flow with minimal perturbations so that the entrained air would flow over the fuel array (Figure 2.4). Tests with multiple lengths of this clear distance seemed to indicate that increasing this distance was slightly correlated with a faster spread rate, but it was later determined that there was insufficient evidence to resolutely confirm this hypothesis. Regardless, an appropriate consistency was achieved with a clear distance of 10 cm, and this length was utilized for all tests within this research project.

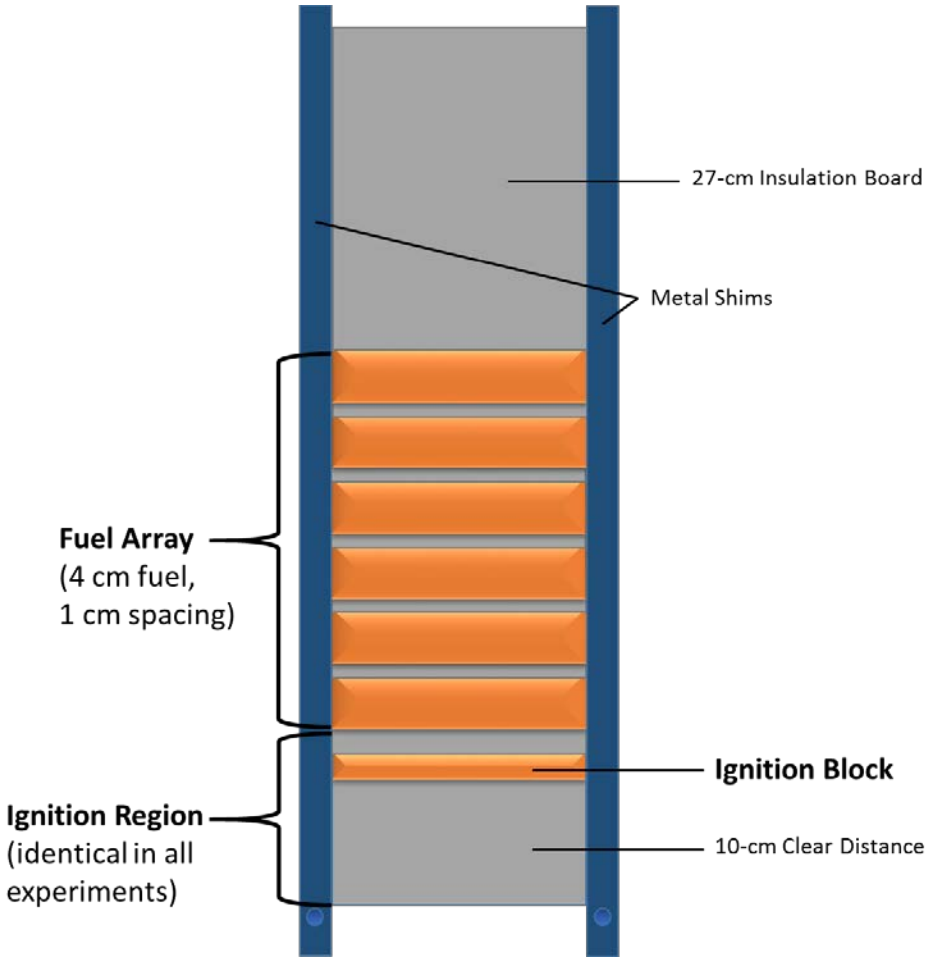

Figure 2.4. Schematic of fuel array configuration for a 4 cm fuel/1 cm spacing test. Only the region demarcated as the fuel array was manipulated between tests.

This first piece of insulation was followed by a block of PMMA that was 2 cm in vertical length. This block of fuel was the ignition source for all experiments, and this 2 cm ignition block was immediately followed by a 2 cm distance of insulation. All experiments retained this same basic structure for the bottommost region of the apparatus in the hope that a certain amount of consistency in ignition and preheating could be retained over multiple tests.

The subsequent fuel array was then varied based on the scenario to be tested. Every fuel array would consist of constant lengths of fuel and insulation, stacked one upon the other in an appropriate pattern. For example, the standard setup in tests of 4 cm fuel and 1 cm spacing is

displayed in Figure 2.4. Note that the fuel-spacing-fuel-spacing pattern is followed within the array until approximately 34 cm from the bottom of the ignition block. All other tests also maintained their respective pattern until approximately 30-35 cm from the bottom of the ignition block was attained. Significant deviations from this fuel array length would skew data comparisons because the pyrolysis front can accelerate as it travels up the apparatus. This consistent array length was therefore maintained to allow for proper comparisons of different tests.

Finally, an insulation board of 27 cm in length was placed on top of the fuel array. This practice was established to maintain a flush experimental surface beyond the fuel so that flame characteristics would not be affected by a sudden change in the vertical surface. Flame height measurements would also deviate if the flush vertical surface was not maintained along the height of the apparatus.

2.5 Experimental Procedure

Preheating of unburnt fuel ahead of the pyrolysis zone can significantly alter ignition times. If inconsistent preheating of the fuel array occurs between tests, inconsistent results for flame spread are a likely manifestation. It was, therefore, of paramount importance that the ignition process be kept consistent and uniform. For our experiments, we elected to minimize the amount of preheating that the fuel array would undergo during the ignition phase. After a multitude of ignition processes were considered and tested, a final design, involving both the ignition of a pilot block of PMMA and the employment of an adequate heat shield, was selected.

The first layer of protection offered by the heat shield consisted in the small sheet of metal that was wedged between the ignition block and the 2 cm insulation above it (see Figure 2.5). As the ignition block was heated, this metal sheet forced hot convective gases away from the apparatus. The metal was more effective at diverting hot gases than any insulative material that was placed against the apparatus. Any insulative material pressed against the apparatus suffered from an air gap, however slight, that would allow some hot gases to push towards higher sections of the fuel array; in contrast, relatively no gases were observed to penetrate the metal sheet wedged directly into the apparatus.

Figure 2.5. Photograph of small sheet of metal wedged between the 2 cm ignition block and the 2 cm piece of insulation above it. This metal shield was meant to keep hot gases away from the virgin fuel during the ignition process.

As a supplement to the metal sheet, a larger shield was leaned against the apparatus above the metal sheet (Figure 2.6). This heat shield consisted of a wooden stand holding a sheet of plywood that would lean against the apparatus at an angle 45° from the vertical. This angular

orientation was established to allow hotter, buoyant gases to naturally vent away from the apparatus. The plywood was also sheathed with a layer of thin metal to prevent any charring or burning during the ignition process. This design proved to be a consistent and effective way to avoid preheating of the fuel array.

Figure 2.6. Photograph of larger shield placed above smaller metal sheet. This wooden construction, which was sheathed in metal, was established to keep hot, convective gases away from the apparatus.

A fully prepped test required that the apparatus, fuel array, mass balance, IR camera, video camera, and heat shield be set into place. Before ignition, the centerline exhaust velocity of the small hood was measured with a hot wire anemometer and recorded. The airflow in the exhaust system could vary significantly due to changes in damper settings at other locations in the laboratory; moreover, the level of exhaust was found to be a probable source of variability in the observed flame spread rates. For this reason, the centerline exhaust velocity was consistently

kept between 2.0 to 2.5 m/s in the 4-inch-radius exhaust opening. Once the centerline velocity was confirmed, the lights in the lab were turned off and the data acquisition systems were activated. 5 seconds after the IR camera started recording, video recording began, and, 10 seconds after the IR camera started, tabulation of the mass data from the load cell commenced. Post-processing of the data easily accounted for these lapses in start-up times.

Once all the data acquisition systems were activated, a blowtorch would be briefly applied to a small ruler made of cardboard and aluminum tape. This ruler was then held adjacent to the apparatus in view of the IR camera, which would detect the difference in emissivity and temperature between the cardboard and aluminum tape. This measuring technique assisted in determination of pyrolysis locations in post-processing.

Finally, two blowtorches were applied directly to the ignition block, above which the heat shield was in place. The blowtorches would be directed onto this PMMA until uniform ignition of the block was achieved. Approximately 15 seconds would elapse from full block ignition, in order to further ensure uniformity of ignition of this PMMA. Subsequently, the heat shield was removed and the flame was allowed to naturally spread up the vertical face of the apparatus.

During the testing, all data acquisition systems would remain active. The test would continue until the mass balance indicated that 100 g had been lost from the original weight of the fuel array. At this point, the flame was extinguished and all acquisition systems were concluded and logged. Data was then transferred and centralized for aggregate post-processing.

2.6 Validation of Infrared Temperature Measurements

Surface temperatures of solid fuels are often measured in fire spread, and these measurements can provide an experimentalist with valuable information. By tracking the temperature contour corresponding to the ignition temperature, an effective pyrolysis front can be tracked. This methodology was undertaken in subsequent analyses.

Initial experimentation was performed with thermocouples and recorded through an NI DAQ infrastructure. The thermocouples were fed through a small hole in the PMMA, bent to lay upon the solid fuel, and melted directly to the surface with a hot metal rod. These thermocouples became unusable after each test, so new thermocouples were needed for each subsequent experiment. However, this process proved incredibly tedious as experimental repeatability necessitated the making and fitting of hundreds of new thermocouples. Moreover, as the PMMA would pyrolyze, thermocouples would occasionally become detached from the surface and extend into the flaming region, artificially raising their temperature. Thermocouples can also only reveal temperature measurements at singular locations along the fuel array. A more desirable method was sought.

Infrared (IR) thermography was a more suitable choice for experimentation. This technique relies on the usage of an infrared camera in measuring the emitted radiation of an object, which is proportional to its absolute temperature. Thermal imaging cameras can also take instantaneous temperature measurements at a wide viewing angle, which makes thermographic data more versatile than point measurements provided by thermocouples.

For our experiment, we were concerned with the temperature of the fuel surface, so it was necessary to filter out confounding effects of flame and soot radiation as much as possible. To minimize flame emissions, many researchers have employed narrow band IR filters to eliminate common emission bands from water, carbon dioxide, and soot [45]. We were able to borrow a FLIR Thermacam SC3000 for our experiment, which operates in the 8-9 μm range. Previously, Urbas and Parker successfully applied an infrared pyrometer in the range of 8-12 μm to measure the surface temperature of burning wood specimens [46]; this was a promising precedent, especially since PMMA should be less affected by soot emissions than burning wood. Validation of our camera's measurements, nonetheless, had to be attempted. Therefore, tests were instrumented with thermocouples and also recorded by the IR camera. After several small-scale tests were conducted, an assumed PMMA emissivity of 0.92 was found to give accurate temperature readings for the infrared images, where accuracy was a measure of similarity to thermocouple values. This value of 0.92 is consistent with the emissivity utilized in transient experiments performed by Sohn et al. [47]. Figure 2.7 displays results from one of the validation tests, in which a linear fit was developed for both the thermocouple data and infrared data. The linear fits are nearly identical; however, it can be clearly seen that the IR data points reflect less scatter than the thermocouple measurements, as evidenced by the R^2-values. Figure 2.8 displays raw data from the same sample validation test where only every other measurement is shown (for graphical clarity). It can be seen that the infrared measurements, which here represented spot measurements, were very close to the thermocouple measurements.

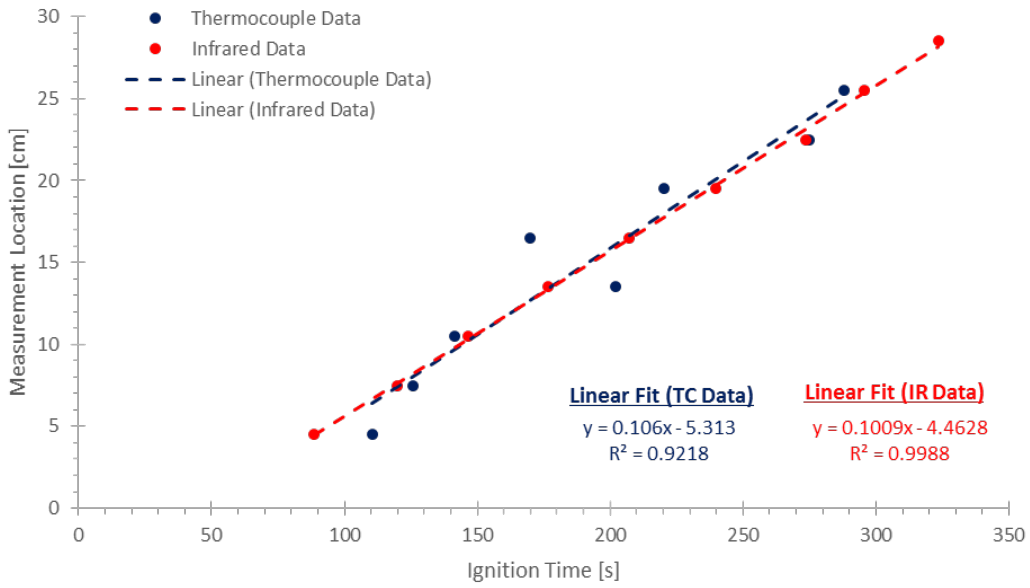

Figure 2.7. Linear fits from thermocouple data and infrared data for a sample validation test. The linear fits from each dataset are nearly identical; however, the TC data exhibits more variability.

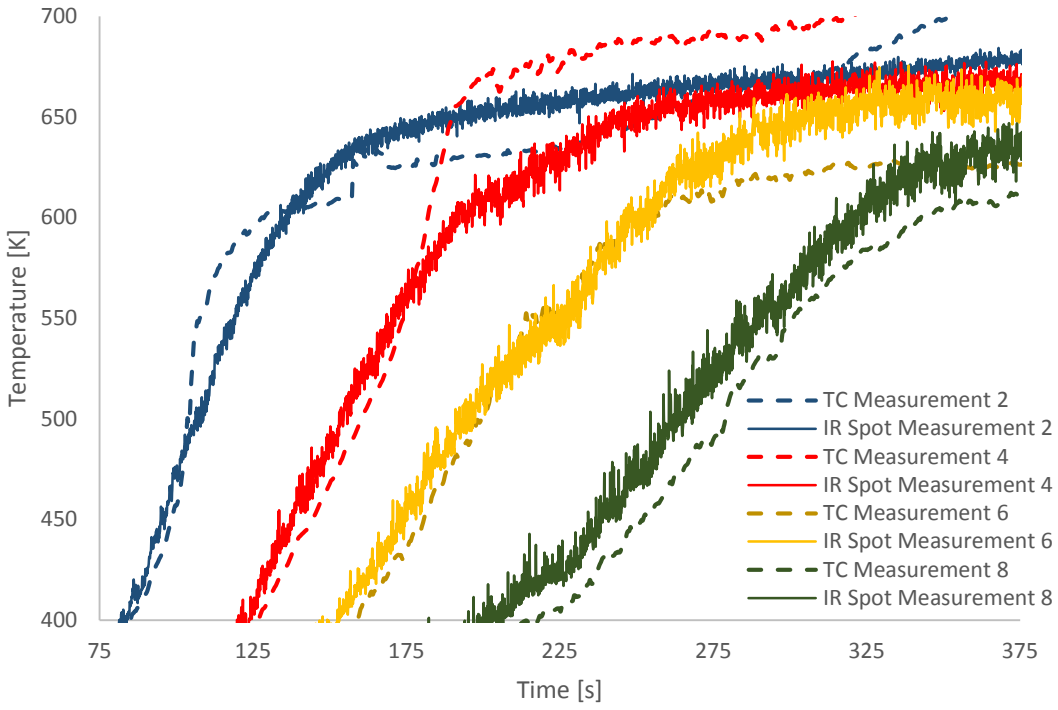

Figure 2.8. Raw data obtained from thermocouples and the infrared camera for a sample validation test.

Infrared thermography was determined to be a more suitable method for our experiments. Smoother overall fits for temperature data were afforded by the infrared images, which did not suffer from the occasional dramatic fluctuations of the thermocouples. It was also more feasible to take more temperature measurements per test, and these measurements were taken from the averages of 2-cm-wide lines along the center of the apparatus (see Figure 2.8). The infrared images provided qualitative and quantitative information that the thermocouples could not. All temperature data referenced in this project are derived from infrared thermography.

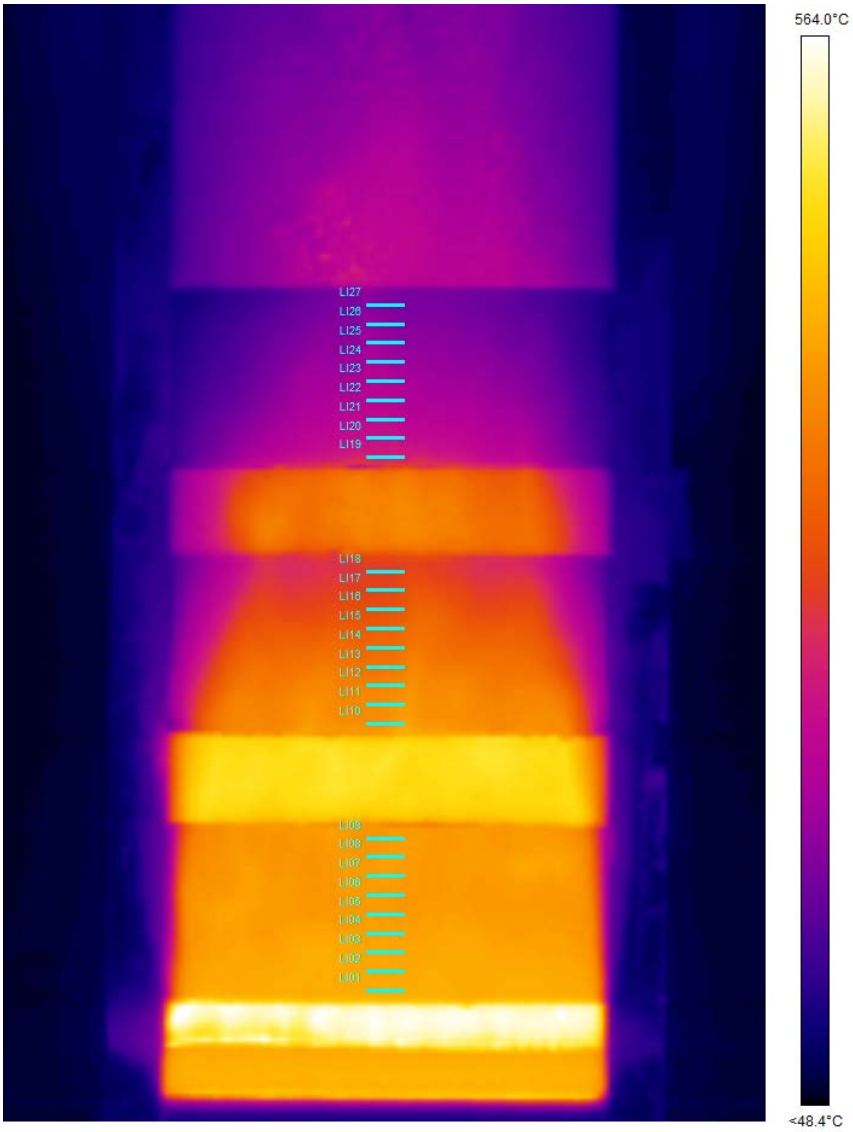

Figure 2.9. Sample infrared image, taken from the spreading phase of 8 cm fuel/4 cm spacing test #2. Note that the horizontal lines along the centerline of the apparatus display the locations of the temperature measurements made by the software during post-processing.

2.7 Flame Height Processing Technique

The pulsations and flickering associated with realistic flames make height measurements complex, and no method of flame height calculation has been generally accepted by the research community as standard practice. In order to avoid any changes in measurement technique between tests, a computerized method was employed in our analyses. Images were captured at 25 fps with a Casio Exilim camera, and the raw video file was converted to an .avi format for MATLAB processing. During this standardized analysis, a user was asked to crop an appropriate section of a still image of the video; this established a representative scale for the remainder of the process. Each frame was then converted to grayscale, and an average gray image was developed from 125 frames (representing a 5 second period). Each pixel in this image was then scanned, with pixels of higher average brightness considered 'activated'; a threshold level of 0.05 was established as the activation level for each pixel in the average gray image. Subsequently, if 10% of the pixels in a horizontal line spanning the fuel array were activated, this line was determined to have a positive flame presence. This litmus test was applied to all horizontal lines spanning the apparatus height. The largest vertical distance with a continuous flame presence was then determined to be the representative flame height. Figure 2.9 illustrates the basic methodology utilized in the flame height calculations, and this process proved repeatable and reliable in all tests when the ambient filming conditions were sufficiently dark.

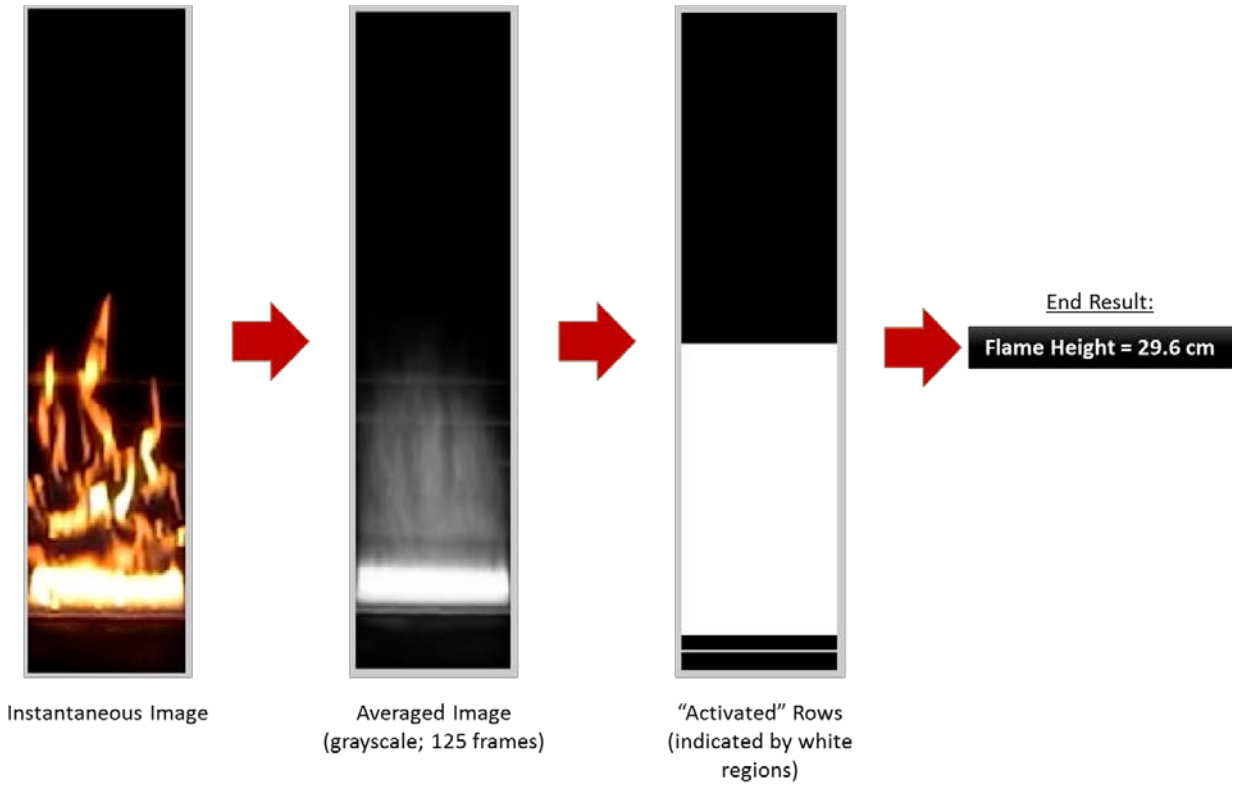

Figure 2.10. Illustration of the methodology used to calculate flame height. All edited images were generated via MATLAB image processing.

2.8 Assumptions and Sources of Experimental Error

The experimental designs possessed several possible sources of experimental error, many of which were mitigated by certain testing practices. One source of variability that was always a valid concern was the ambient air flow, which could affect the entrainment patterns of the test. As stated before, the exhaust airflow was kept at a constant, low velocity in an effort to minimize inconsistency between tests. Additionally, the ignition block of PMMA was always placed on top of a 10-cm-tall piece of insulation; this strategy was meant to alleviate strange behavior from the tripping of the boundary layer. Experimental testing seemed to imply that the airflow and boundary layer development could play a significant role in the results. An extensive analysis of

the roles of these variables was beyond the scope of this study; instead, the aforementioned methodologies were established to lessen variability between tests as much as reasonably possible.

The consistency of the properties of the PMMA could also affect results. Fortunately, the behavior of the cast PMMA under slight changes in ambient temperature or humidity did not appear to be a concern. As the PMMA undergoes physical changes related to pyrolysis, the surface emissivity changes; nevertheless, our results were only concerned with the emissivity value at the onset of pyrolysis. This emissivity was verified through testing. Deformation of the PMMA was a definite concern, as heating would weaken the rigidity of the blocks and they would begin to sag. The sagging effects were eliminated by increasing the thickness of the PMMA slabs to 1.27 cm. This thickness also provided enough fuel to avoid any stages of burnout during the spreading phases of all tests (with the exceptions of the limiting cases). Lastly, conduction of heat from the aluminum shims to the fuel was found to be negligible (verified through IR images).

The repeatability of ignition is a significant source of concern in upward flame spread experiments. If the ignition process leads to more preheating of the virgin fuel up the apparatus in a certain test, the flame spread rate could be artificially accelerated. Furthermore, if the ignition is not uniform, heating effects may be skewed towards one side of the apparatus which would change the shape of the advancing pyrolysis front. The ignition process of this study appeared to mitigate these concerns adequately.

Because the measurements for the height of the pyrolysis zones were taken at the centerline, the shape of the pyrolysis front is also a source of concern. Non-uniform spreading may lead to an inaccurate estimation of the location of the pyrolysis front. In order to promote a

more uniform spread rate, a fuel width (20 cm) was selected based on the recommendations of previous researchers [25, 27]. Later analysis, detailed in Section 4.3, indicates that the pyrolysis front maintained the same basic U-shape during all tests. This shape implies that the true pyrolysis height is not uniform across the apparatus; regardless, the consistency of temperature measurement along the centerline allowed for proper comparison of trends between tests.

The sizing and flushness of the insulation and PMMA was always a source of some variability. Slight discrepancies in height of these pieces existed as an unavoidable consequence of manual cutting and sizing, but these incongruities were marginal at most. The pieces of insulation were always slightly thicker than the PMMA pieces, which consistently affected the flushness of the fuel array. These slight perturbations seemed to play at least a minor role in the flame spread process. The homogeneous tests had only one perturbation along the fuel array at $x = 25\ cm$, but in two out of three tests, the effect of this subtle change was visible in a plot of $x_{p,total}$ vs. time (Figure 2.10). These perturbations related to the flushness of the fuel array would increase in number for arrays with lots of fuel-to-insulation transitions. This phenomenon likely manifested itself in the discrete tests of 4 cm and 8 cm fuel, but the overall trends and fits glossed over these perturbations adequately. Tests of 2 cm fuel were also considered before being tossed out due to inconsistent results, likely a manifestation of the large number of perturbations inherent to these fuel arrays.

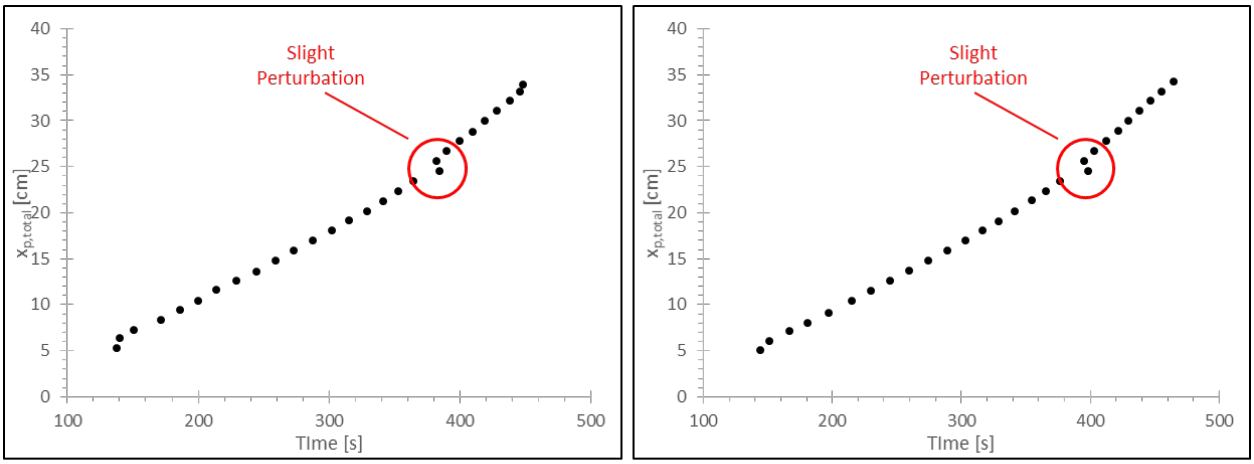

Homogeneous Test # 1

Homogeneous Test # 2

Figure 2.11. A slight perturbation existed in the homogeneous tests at 25 cm (the full slab had to be cut across its width at this location and reassembled in order to fit into the apparatus). This blemish resulted in a visible perturbation in the plots for two out of the three homogeneous tests.

Chapter 3: Experimental Results

3.1 Flame Spread Rate

The foremost objective of this study was to look at the effect of different discrete fuel arrays on the flame spread rate, V_p. V_p is the rate at which the pyrolysis front moves across the fuel array. For discrete fuels, calculations of flame spread velocity have to account for the spacing in between the fuels; these spacings lead to discontinuities that are not witnessed in the traditional flame spread problem. Recall that, for this reason, a new velocity, the fuel spread rate, or $V_{p,fuel}$, was also established. This fuel spread rate is calculated by ignoring the inert regions of the spacings and looking only at the vertical distance of fuel consumed, $x_{p,fuel}$. We investigated V_p and $V_{p,fuel}$ for all test cases.

In order to determine V_p and $V_{p,fuel}$, the pyrolysis height $x_{p,total}$, the distance between the advancing pyrolysis front and the bottom of the ignition block, had to be quantified. $x_{p,total}$ was calculated under the conjecture that the pyrolysis temperature was 300°C, an assumption that has been utilized by previous experimentalists [21, 24]. This postulation enabled the following measurement technique: As the flame traversed the fuel array, infrared thermography captured average temperatures at representative 2-cm-wide sections along the centerline of the apparatus. The derived temperature data was then smoothed by means of a polynomial fit; subsequently, the intersection of this fit with 300°C was established as the ignition time for each respective height. These ignition times represent the instants at which the pyrolysis front has reached a certain height. Given these ignition times, flame spread rates could then be determined by

applying a linear fit to each test. Two linear fits were applied: a total linear fit was applied to points along the entire height of the fuel array to determine a total flame spread rate; another linear fit was applied to the middle portion of the fuel array (i.e. between 10 and 25 cm in height) in order to determine a representative flame spread rate (Figure 3.1). An example of both of these linear fits is displayed in Figure 3.2. We opted to employ the representative linear fit in *all* subsequent analyses. We discarded the total linear fit under the impression that a representative spread rate could better capture the effects intimately connected with the fuel arrangement. The usage of a middling linear fit mitigated variability from early and later phases of spread. The lower region of the fuel array was more affected by the ignition source, and it was also exposed to a flame that has not transitioned from the laminar state. Meanwhile, the upper region of the fuel array exhibited greater acceleratory effects. For these reasons, all reported flame spread rates have been calculated from the representative region of the fuel array (10 to 25 cm in height). Slight expansions of this region (approximately 2-3 cm) were made on fuel arrays where more data points were desired.

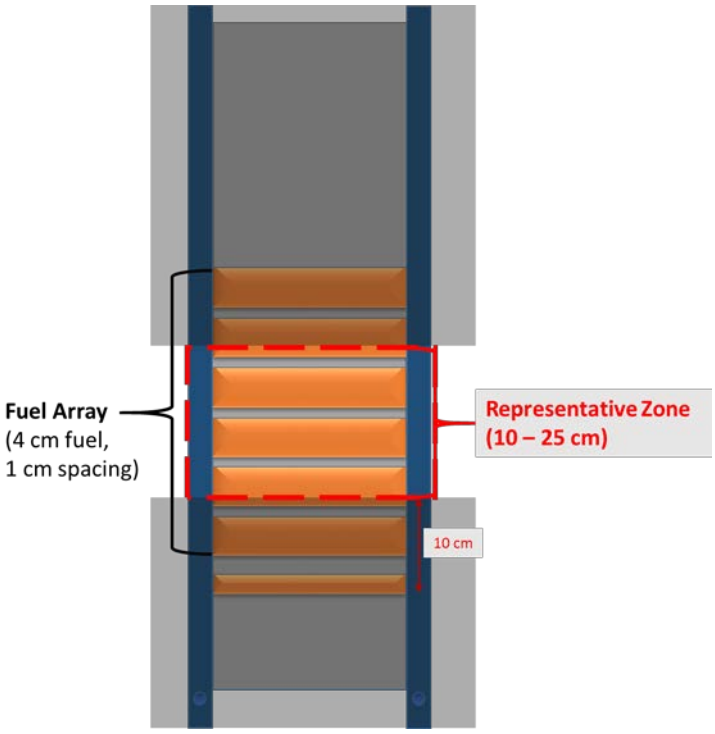

Figure 3.1. The red box in the above diagram provides an example of the middle region used to obtain a representative flame spread rate.

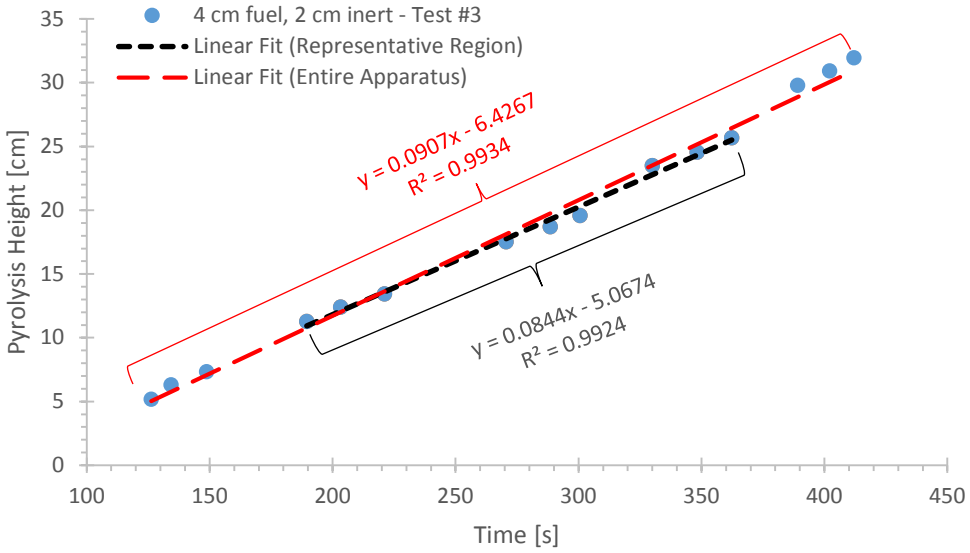

Figure 3.2. Pyrolysis Height vs. Time for a sample experiment (4 cm fuel, 2 cm inert – Test #3). The red linear fit displayed represents a total linear fit, which was calculated using points along the entire fuel array. The black linear fit is a representative linear fit, which is a measure of the middle 10-25 cm of the apparatus. The representative linear fit was used in all spread rate calculations.

Once 3 to 4 individual tests with identical fuel array patterns (i.e., same fuel length and spacing) were completed, a flame spread rate for the discrete fuel array was determined by averaging V_p from all identical experiments. The fuel percentage of the array was then used to compare results from different discrete fuel arrays. The fuel percentage is simply the hypothetical percentage of the array surface area consisting of exposed fuel. For example, a test with 4 cm slabs of fuel and 1 cm spacing would possess a fuel percentage of [(4 cm fuel)/(4 cm fuel + 1 cm spacing) = 80%]. This quantity succinctly reveals the basic structure of the discrete fuel array.

Subsequently, the flame spread rates V_p and the fuel spread rates $V_{p,fuel}$ were plotted against fuel percentages. Both V_p and $V_{p,fuel}$ for the homogeneous tests (i.e., tests with full slabs of PMMA and no spacing) exhibited minimal variability between experiments; additionally, these points provided baseline velocities against which the discrete fuel cases could be readily compared. Variability of V_p and $V_{p,fuel}$ was higher in the discrete fuel arrays, as indicated by the error bars. In the rare case that a test exhibited a spread rate that was beyond 2 standard deviations from the mean of other identical tests, it was discarded. The flame spread velocity for the full slab test was 0.080 cm/s, which is reasonably close to the value of 0.075 cm/s obtained by Pizzo et al., who also studied 20-cm-wide vertical PMMA [9].

Plotting flame spread rate vs. fuel percentage provides perhaps the most intuitive quantification of results. For 4 cm slabs of fuel (Figure 3.3), the spread rate slowly starts to increase from the homogeneous case as spacing is slowly increased. This spread rate peaks at around a 67% fuel composition, in the scenario where 2 cm spacing was employed. This represents the optimal spread rate configuration for fuel arrays with 4-cm-tall PMMA. As the fuel percentage is lowered from this optimal configuration, a significant decline in spread rate is

observed. 4 cm spacing tests, representing a fuel composition of 50%, exhibit a spread rate that is 0.05 cm/s slower than the homogeneous case. This trend of decreased speed with increased spacing should continue until a threshold value is reached, upon which flames will no longer successfully spread up the apparatus.

The flame spread rate for 8 cm slabs of fuel exhibit a very similar trend as the 4 cm slabs of fuel. For the 8 cm slabs (Figure 3.4), the flame spread rate is highest at fuel percentages of 89%, 80%, and 67%, all of which hover around 0.09 cm/s. These tests represent the scenarios where 1 cm, 2 cm, and 4 cm spacings were employed. In the two remaining scenarios, comprising fuel percentages of 50% and 40%, a significant decline in the spread rate is observed. In all likelihood, this decrease in flame spread rate will continue as the fuel percentage is increased until there is no spread up the apparatus.

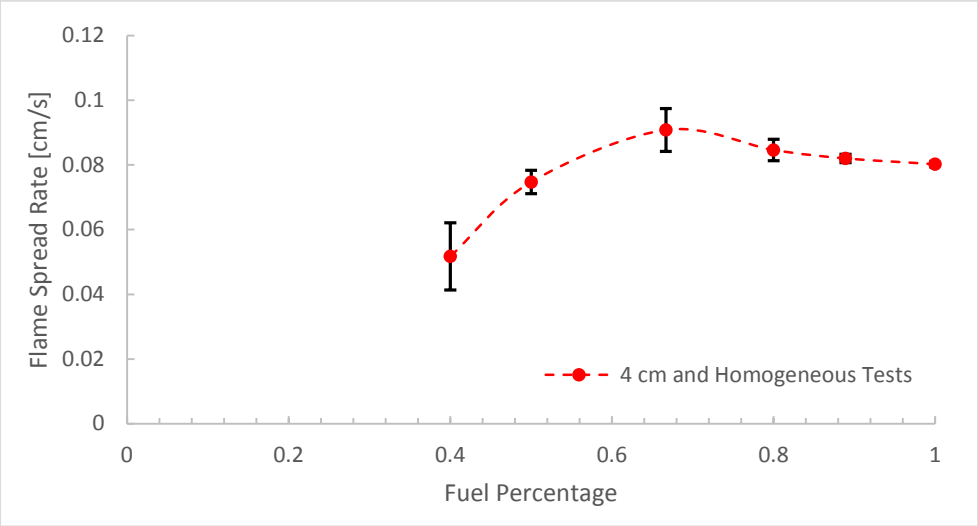

Figure 3.3. Flame spread rate vs. fuel percentage for the 4 cm and homogeneous tests.

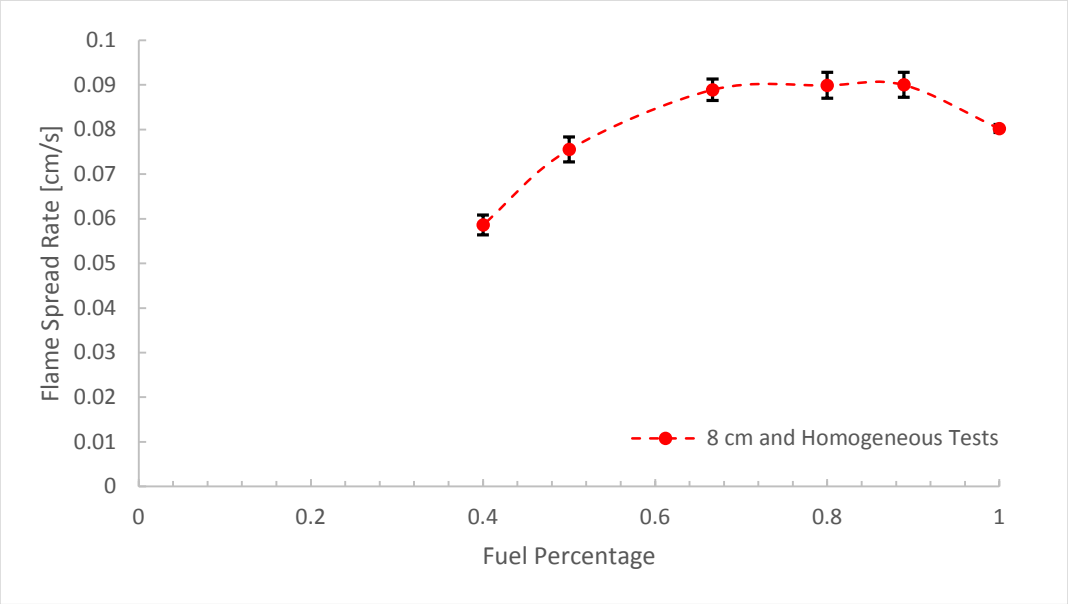

Figure 3.4. Flame spread rate vs. fuel percentage for the 8 cm and homogeneous tests.

The fuel spread rate is also a function of the fuel percentage. As the percentage of fuel in the array increases, $V_{p,fuel}$ increases. This trend is observed for all points in both the 4 cm fuel and the 8 cm fuel tests, as shown in Figures 3.5 and 3.6. A maximum fuel spread velocity is attained for the homogeneous tests at 0.080 cm/s, which is necessarily the homogeneous flame spread rate as well. Both the 4 cm fuel and 8 cm fuel tests exhibit a minimum fuel spread velocity of 0.019 at a fuel percentage of 40%. The positive correlation of fuel spread rate with fuel percentage appears remarkably consistent across all tests.

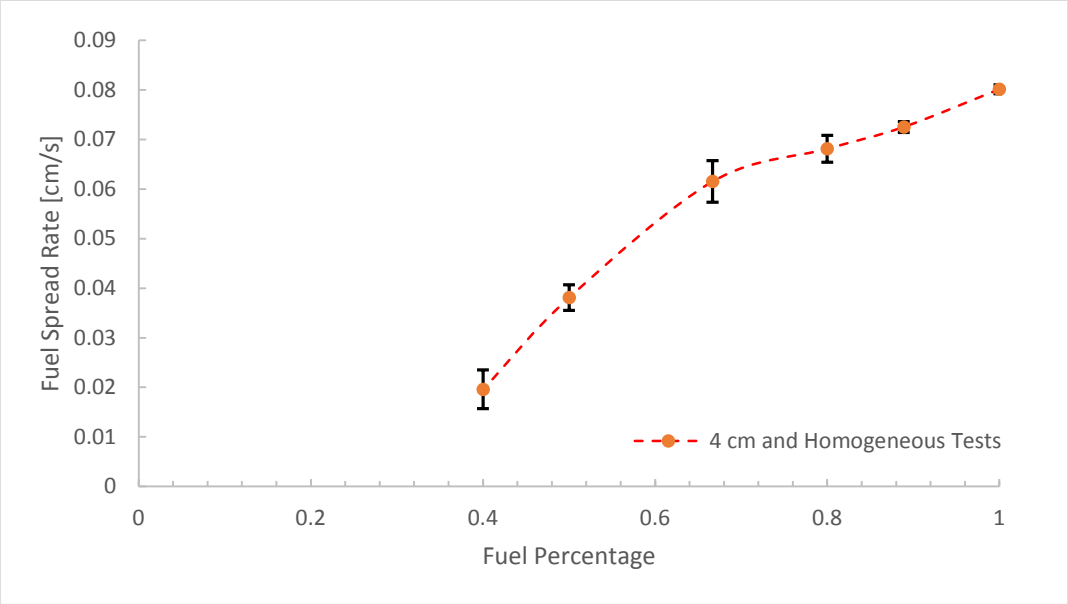

Figure 3.5. Fuel spread rate vs. fuel percentage for the 4 cm and homogeneous tests.

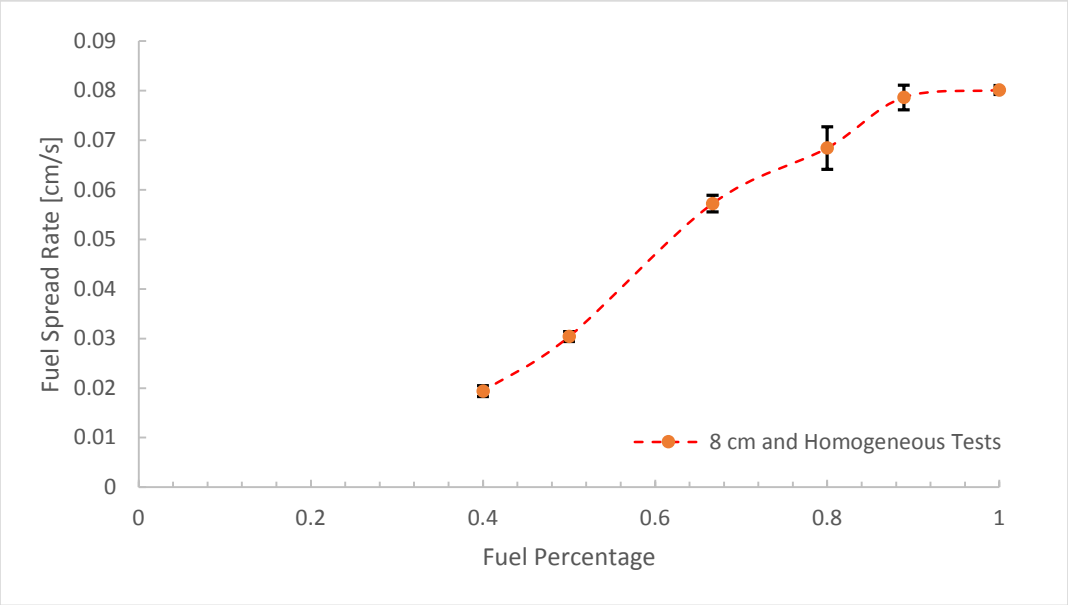

Figure 3.6. Fuel spread rate vs. fuel percentage for the 8 cm and homogeneous tests.

Figures 3.7 and 3.8 display the fuel and flame spread rates vs. fuel percentage for the 4 cm fuel tests and the 8 cm tests, respectively. For the homogeneous tests, representing a fuel

percentage of 100%, the flame spread rate necessarily coincides with the fuel spread rate. For all other tests, the fuel spread rate is necessarily less than the flame spread rate.

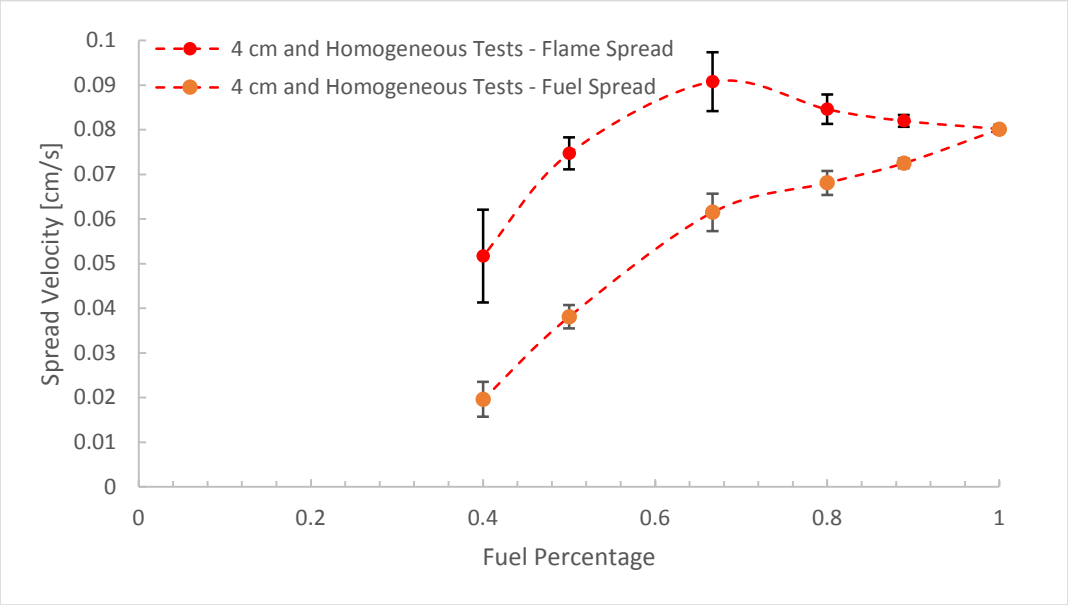

Figure 3.7. Comparison of the flame spread and fuel spread rates vs. fuel percentage for the 4 cm and homogeneous tests.

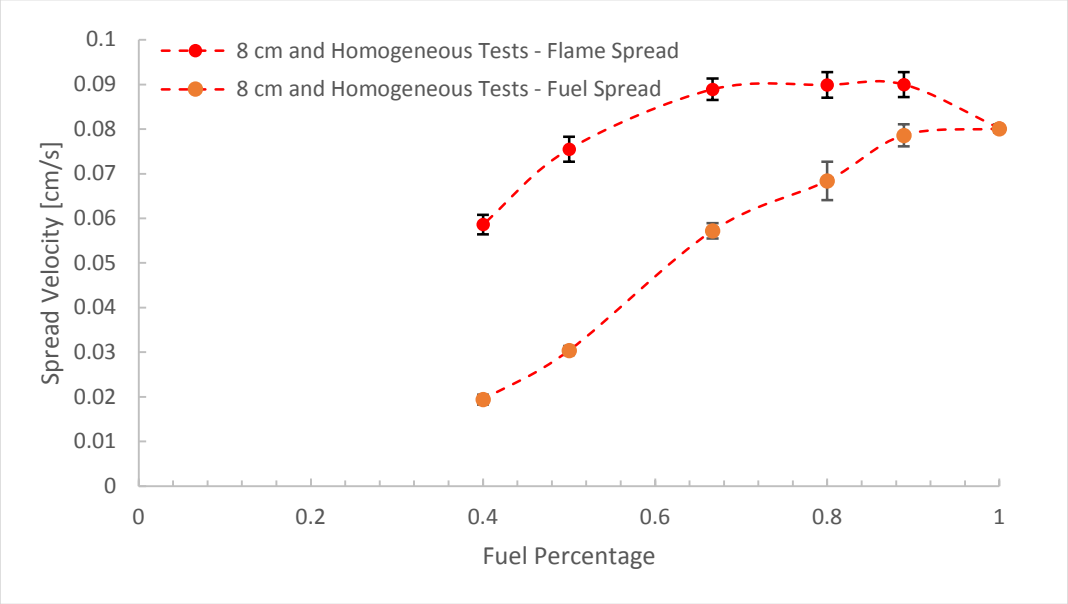

Figure 3.8. Comparison of the flame spread and fuel spread rates vs. fuel percentage for the 8 cm and homogeneous tests.

3.2 Mass Loss Rate

Mass loss rates for each test were determined from the mass loss data. By eliminating outliers and applying an 8th-order polynomial fit, the mass loss rates for each test were determined. As a comparison of calculation methods, Figure 3.9 displays an example of this computed mass loss rate vs. an 11-point simple moving average.

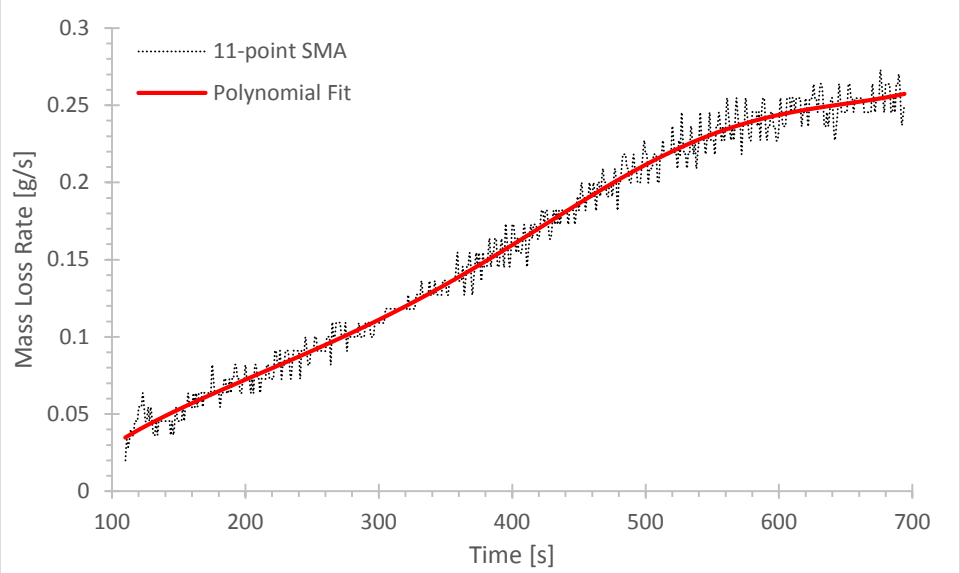

Figure 3.9. Results for the mass loss rate vs. time from a sample test (4 cm fuel, 2 cm inert – Test #3). An 11-point simple moving average is compared against the polynomial fit that was used in the analysis.

In order to compare the mass loss rates at various times of the test, the starting point for every test was normalized as the point when the first temperature measurement of the fuel array reached the pyrolysis temperature (300°C). For matching fuel array configurations, mass loss rates from each experiment were averaged to develop representative mass loss rates.

Figure 3.10 displays mass loss rates for the homogeneous case and 4 cm fuel tests. All tests exhibit comparable mass loss rates for the first 200 seconds, increasing from 0.05 g/s to 0.11

g/s. After this point, the mass loss rate for the 4 cm spacing is outpaced by all the other tests. Eventually, every other test also becomes outpaced by the homogeneous case.

Figure 3.11 displays mass loss rates for the homogeneous case and 8 cm fuel tests. Similar to the 4 cm fuel results, all tests exhibit comparable mass loss rates for the first 200 seconds. After this point, the mass loss rates remain highest for the tests with minimal spacing.

The mass loss rate for all tests exhibit consistently positive slopes, indicating that the steady burning period has not yet been reached. Nevertheless, the negative concavity of each mass loss rate towards the latter period of all tests indicate that a steady mass loss rate is being approached after the completion of spread.

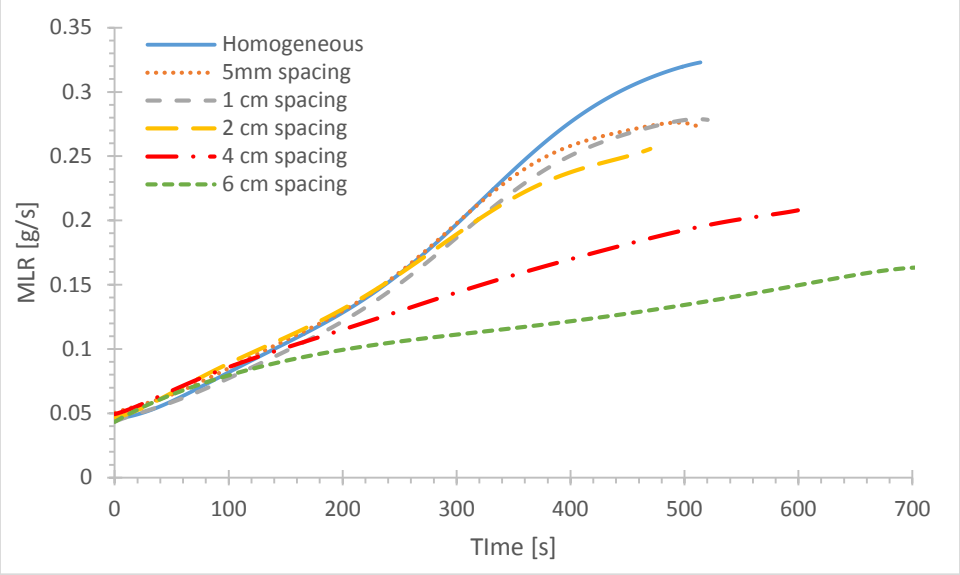

Figure 3.10. Mass loss rate vs. time for all 4 cm fuel tests and the homogeneous tests.

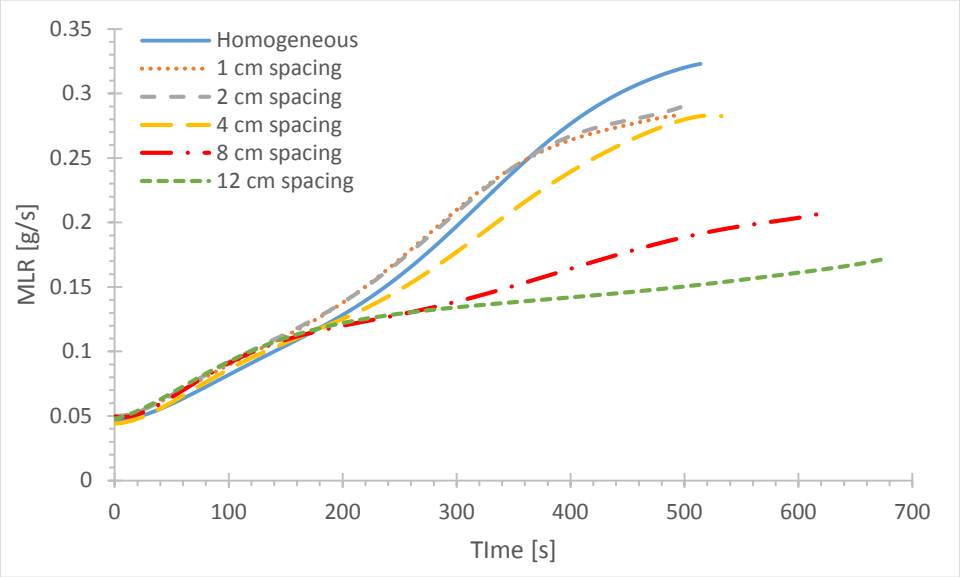

Figure 3.11. Mass loss rate vs. time for all 8 cm fuel tests and the homogeneous tests.

3.3 Flame Height

Flame heights for each test were computed from video footage via MATLAB processing. An 8th order polynomial fit adequately smoothed flame height test data (see example in Figure 3.12). Similar to the mass loss rates, a normalized start time was developed based on the time when the lowest temperature measurement reaches the pyrolysis temperature (300^{o}C).

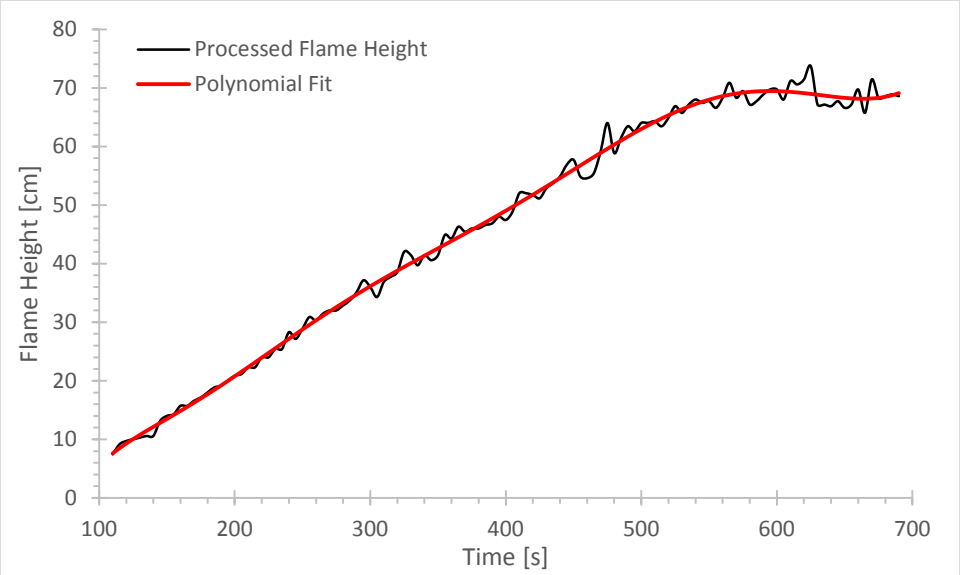

Figure 3.12. Results for the flame height vs. time from a sample test (4 cm fuel, 2 cm inert – Test #3). The processed flame height was smoothed by means of an 8th order polynomial fit.

Flame heights vs. time are plotted in Figures 3.13 and 3.14 for the 4 cm fuel tests and the 8 cm fuel tests. The homogeneous case is included in both figures. For the first 200 seconds, flame heights for all tests are nearly the same, increasing from 12 to 37 cm in height. After this, some tests exhibit a decrease in the rate of increase of flame spread, beginning with the largest spacing. By 400 seconds, the homogeneous case possesses the largest flame height. Towards the latter end of data acquisition, the flame heights for the 4 cm fuel tests appear to correlate positively with the fuel percentage. The 8 cm fuel results appear to have a slight positive correlation of flame height to fuel percentage, but the correlation is somewhat messier.

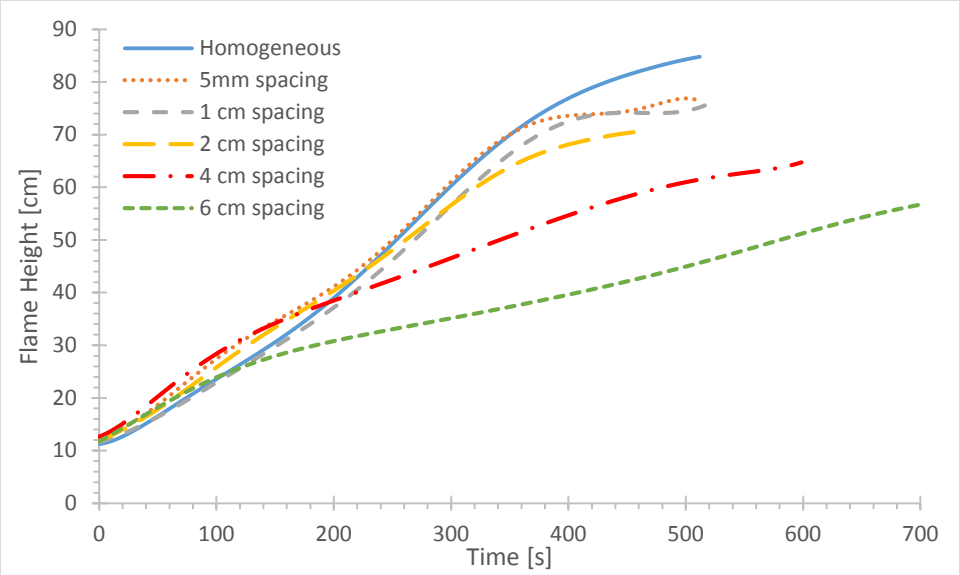

Figure 3.13. Flame heights vs. time for the 4 cm fuel and homogeneous tests.

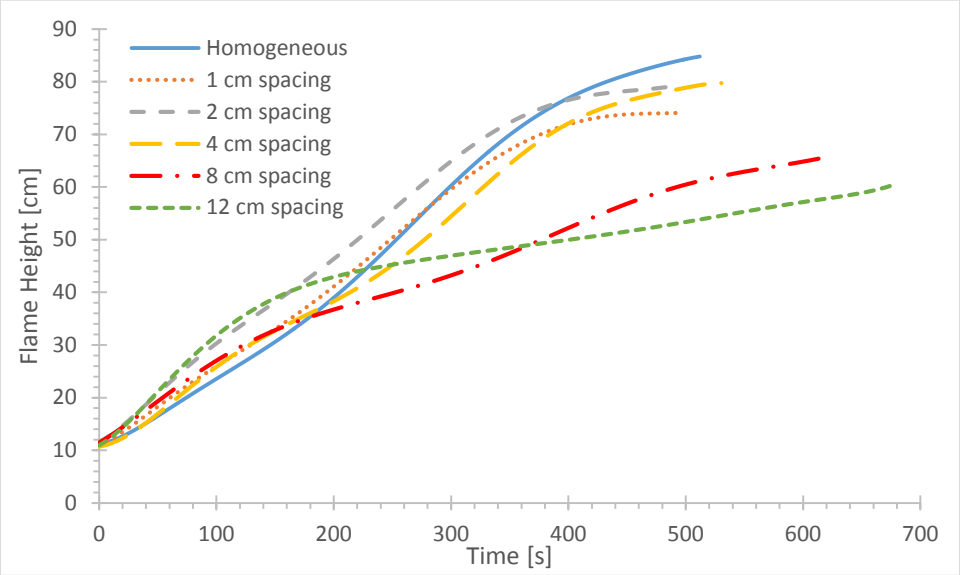

Figure 3.14. Flame heights vs. time for the 8 cm fuel and homogeneous tests.

3.4 Pyrolysis Height

For each fuel array configuration, representative flame spread and fuel spread velocities, V_p and $V_{p,fuel}$, respectively, were averaged from each test to develop estimates of the total

pyrolysis height, $x_{p,total}$, and the fuel pyrolysis height, $x_{p,f}$. To develop these estimates, a linear fit was applied, where $t = 0$ was established as the time when the lowest temperature measurement reached the pyrolysis temperature (300°C). This linear fit was capped at 0.5 cm above the highest temperature measurement location, which is approximately equivalent to the end of the fuel array. Although these estimates do not account for the acceleration of the pyrolysis front, the results proved adequate for most subsequent calculations, such as the mass loss rate per unit area. Figures 3.15 – 3.18 display graphs of $x_{p,total}$ and $x_{p,f}$ vs. time for 4 cm and 8 cm fuel.

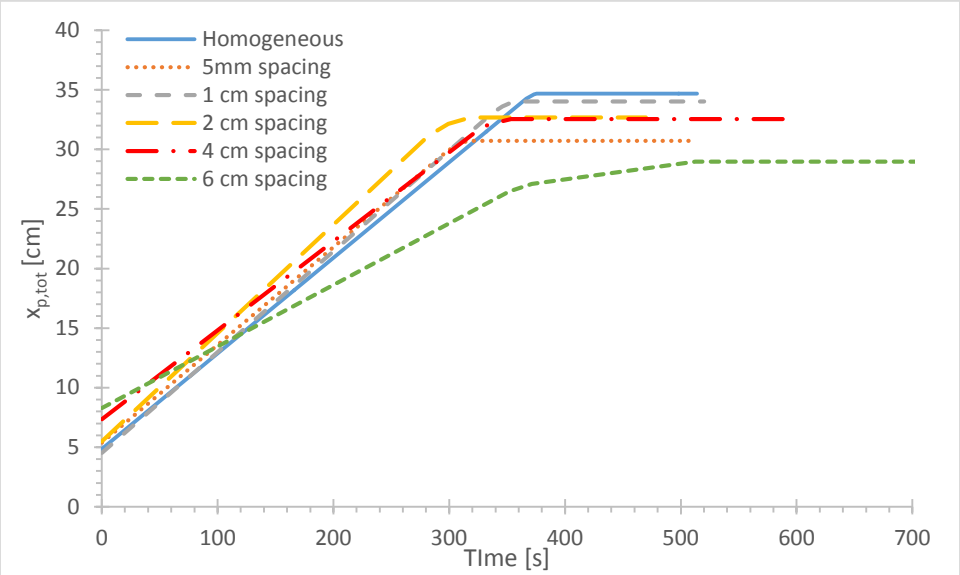

Figure 3.15. Total pyrolysis heights vs. time for the 4 cm fuel and homogeneous tests.

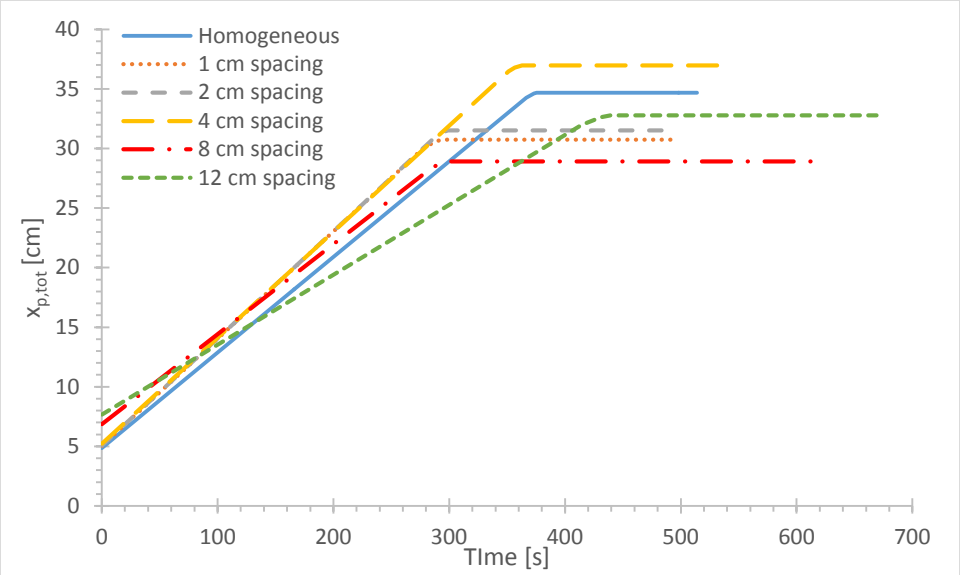

Figure 3.16. Total pyrolysis heights vs. time for the 8 cm fuel and homogeneous tests.

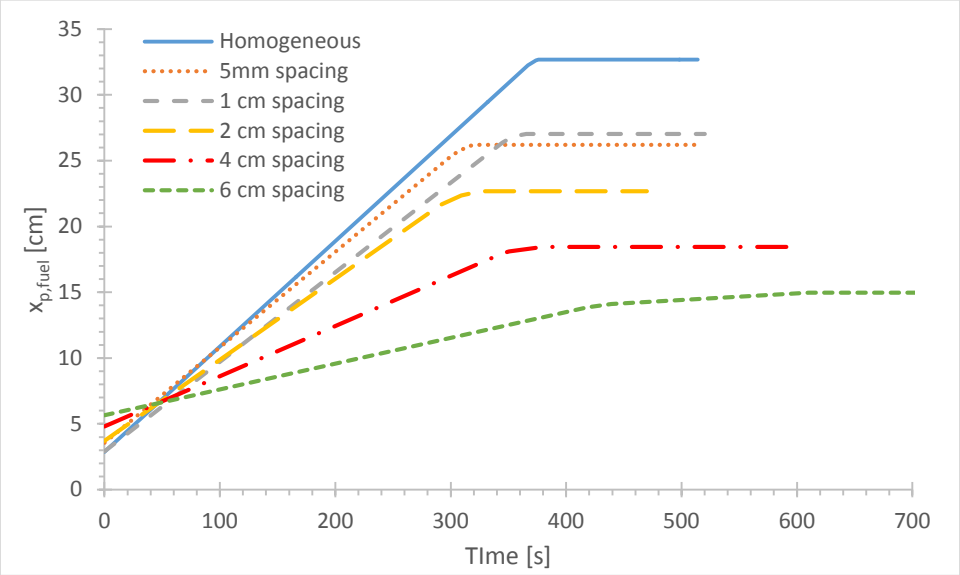

Figure 3.17. Fuel pyrolysis heights vs. time for the 4 cm fuel and homogeneous tests.

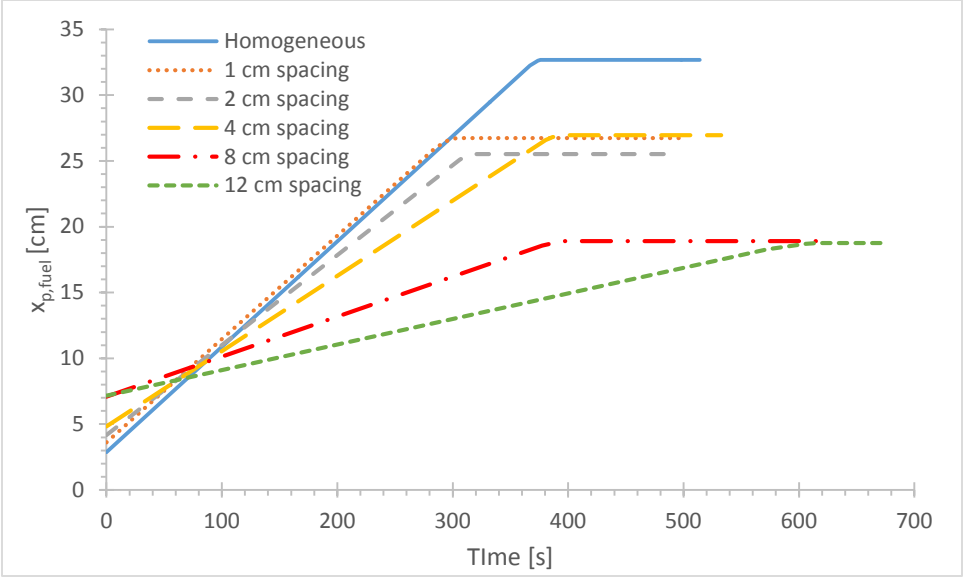

Figure 3.18. Fuel pyrolysis heights vs. time for the 8 cm fuel and homogeneous tests.

3.5 Mass Loss Rate per Unit Area

The mass loss rate per unit area, $\dot{m}''$, was obtained from the mass loss rate and the pyrolysis heights using the following methodology. Two measures of this mass flux were obtained: the mass loss rate per total pyrolysis area ($\dot{m}''_{total}$) and the mass loss rate per burning area ($\dot{m}''_{fuel}$). Equations 3.1 and 3.2 demonstrate how these parameters were calculated:

$$\dot{m}''_{total} = \frac{\dot{m}}{(20\ cm \cdot x_{p,total})} \tag{3.1}$$

$$\dot{m}''_{fuel} = \frac{\dot{m}}{(20\ cm \cdot x_{p,fuel})} \tag{3.2}$$

where $x_{p,total}$ and $x_{p,fuel}$ estimates were derived from the pyrolysis heights.

Figure 3.19 displays an example result for a test with 4 cm fuel and 2 cm spacing. The slight cusp around 450 seconds is indicative of the approximate time where the flame front reached the top of the apparatus.

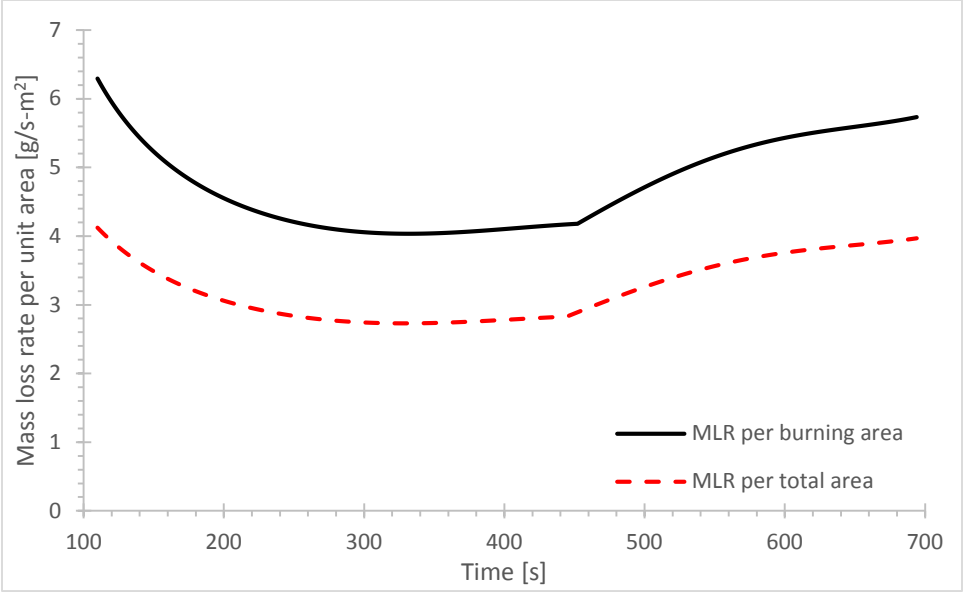

Figure 3.19. Results for $\dot{m}"_{fuel}$ and $\dot{m}"_{total}$ vs. time from a sample test (4 cm fuel, 2 cm inert – Test #3).

There are important differences between $\dot{m}"_{fuel}$ and $\dot{m}"_{total}$. $\dot{m}"_{fuel}$ is the true burning mass flux, for this parameter quantifies a burning area by neglecting the inert sections of the fuel array. Meanwhile, $\dot{m}"_{total}$ quantifies an average mass flux for a given area. Therefore, only the homogeneous case possesses identical values of $\dot{m}"_{fuel}$ and $\dot{m}"_{total}$. For all other arrays, $\dot{m}"_{fuel}$ is necessarily greater than $\dot{m}"_{total}$.

Figures 3.20 and 3.21 display plots of $\dot{m}"_{total}$ vs. time for the 4 cm fuel and homogeneous cases as well as the 8 cm fuel and homogeneous cases. Most experiments in this dataset exhibit a high initial mass flux followed by a sharp decline. The high initial mass flux occurs because at this point only the ignition block and a small portion of the fuel array has ignited. Because the ignition block is always entirely ignited before the heat shield is removed, a significant mass flux has developed across the entire breadth of the apparatus. Video footage reveals images of a bright, constant, laminar flame above the ignition block as soon as the heat shield is removed

(Figure 3.22). As the pyrolysis height increases, however, the beginning stages of spread don't exhibit this same uniformity. The flame spread rate is measured along the centerline, where the pyrolysis front advances fastest; consequently, the burning area employed to compute $\dot{m}''_{total}$ is overestimated by including the edges where the pyrolysis front lags slightly behind. Additionally, video footage reveals a transition from a distinctly uniform, laminar flame to a more V-shaped, turbulent flame for the middle/upper regions of the apparatus in the spreading phase (Figure 3.22). These factors result in the valley observed in the plot of $\dot{m}''_{total}$ during the middle phases of the flame spread. As the pyrolysis front moves to the upper portions of the apparatus, $\dot{m}''_{total}$ recovers and increases. This is the expected result along the fuel array at a mature stage in flame spread; it is at this point where the thermal wave is penetrating deeper layers of the PMMA and increasing the average temperature of the PMMA. Moreover, a fuller portion of the width is involved in pyrolysis. This uniformity of pyrolysis along the breadth of the apparatus mitigates the edge effects that contributed to the initial overestimation of burning area. For the aforementioned reasons, $\dot{m}''_{total}$ rises again, and the generally negative concavity of this parameter in the late stages of the test indicate a steady value is being approached.

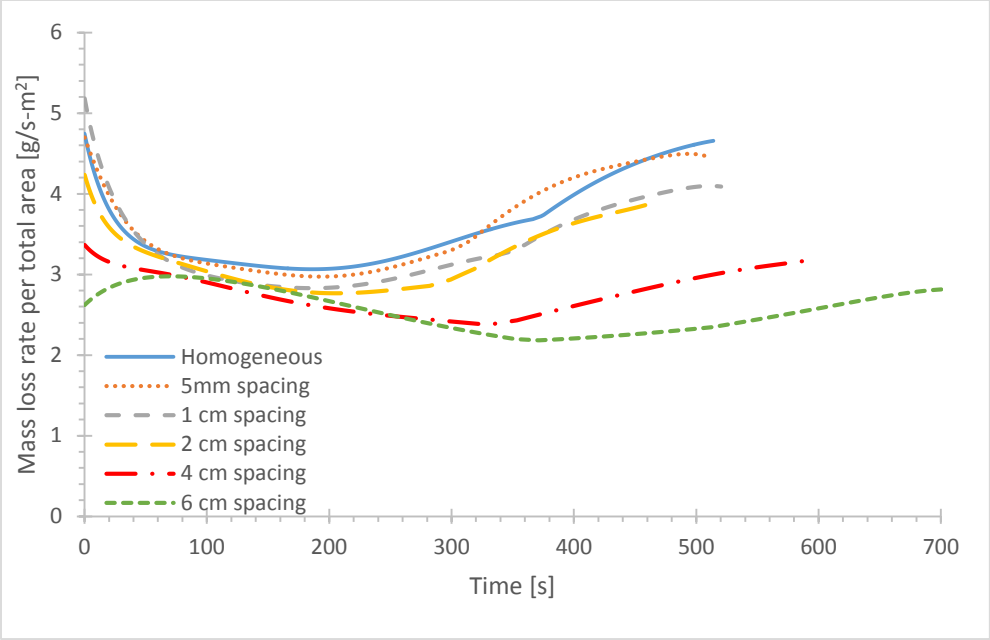

Figure 3.20. $\dot{m}''_{total}$ vs. time for the 4 cm fuel and homogeneous tests.

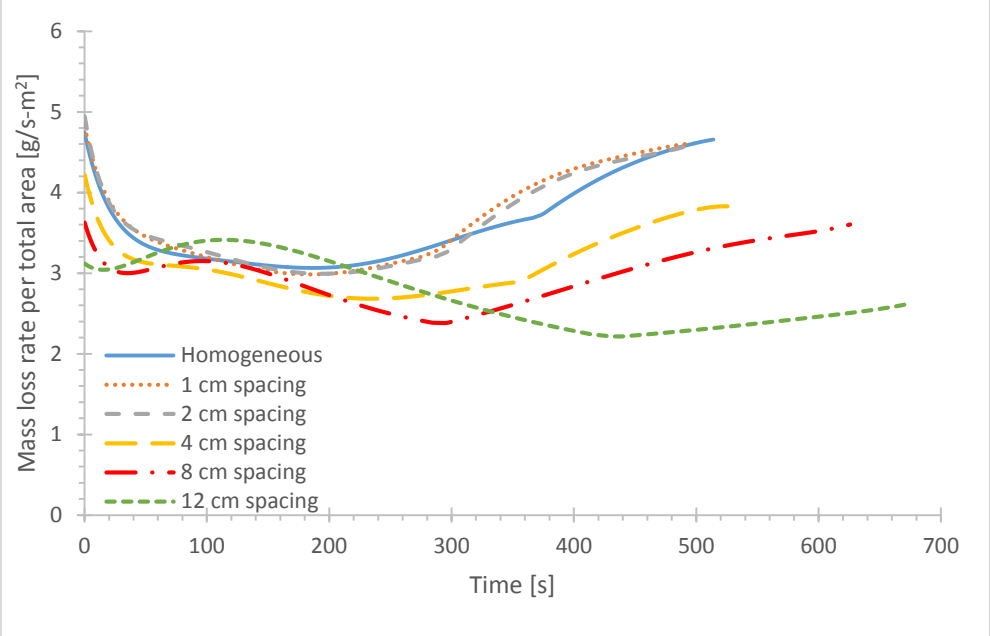

Figure 3.21. $\dot{m}''_{total}$ vs. time for the 8 cm fuel and homogeneous tests.

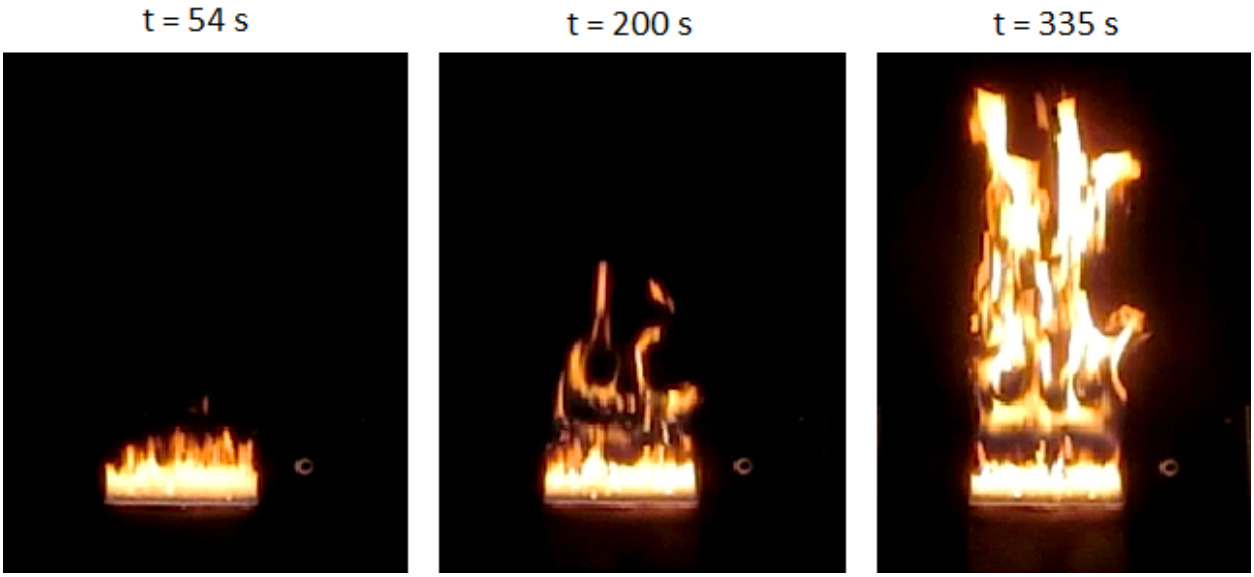

Figure 3.22. Stages of flame spread for a sample test (full slab test #2), in left-to-right chronological order. At the beginning of the test a steady, uniform, laminar flame is seen. In the middle phases of flame spread, turbulent structures form in a slightly V-shaped flame. At the latter phases of testing, a developed burning area leads to a flame that fully engulfs the fuel array. To match the normalized times of the reported data, all displayed times have been normalized by setting the starting point for the test as the point when the first temperature measurement of the fuel array reached the pyrolysis temperature (300°C).

Figures 3.23 and 3.24 display plots of $\dot{m}"_{fuel}$ vs. time for the 4 cm fuel and homogeneous cases as well as the 8 cm fuel and homogeneous cases. The general trend for these experiments is nearly the same as that of $\dot{m}"_{total}$: the high values initially observed for $\dot{m}"_{fuel}$ can be explained by the uniform, developed burning of the ignition block; the low values observed during the middle spreading period are consequences of an overestimation of the burning area and the immature stages of thermal penetration; the resurgence of values is a result of a more developed burning region across nearly the entire fuel array.

The exceptions to the aforementioned trends are the tests with the lowest fuel percentages, namely the 4 cm fuel/6 cm spacing, the 8 cm fuel/8 cm spacing, and the 8 cm fuel/12 cm spacing arrays. In contrast to the other tests, $\dot{m}"_{fuel}$ and even $\dot{m}"_{total}$ actually peak towards the middle

period of spreading. This is a consequence of the linear fit for the pyrolysis height that was used in calculation of these mass fluxes. In reality, the progression of the pyrolysis front for tests with significant spacing is non-linear: as soon as the pyrolysis front encounters the large distances of inert material along these arrays, it must halt. At this point, the location of the pyrolysis front remains stagnant while the closest block of fuel slowly heats up to its ignition temperature. Once this ignition temperature is reached, the pyrolysis front will begin to advance across the next block of fuel. It is this 'jumping' phenomenon, which is observed in tests with low fuel percentages, that complicates approximations of $\dot{m}"_{fuel}$ and $\dot{m}"_{total}$.

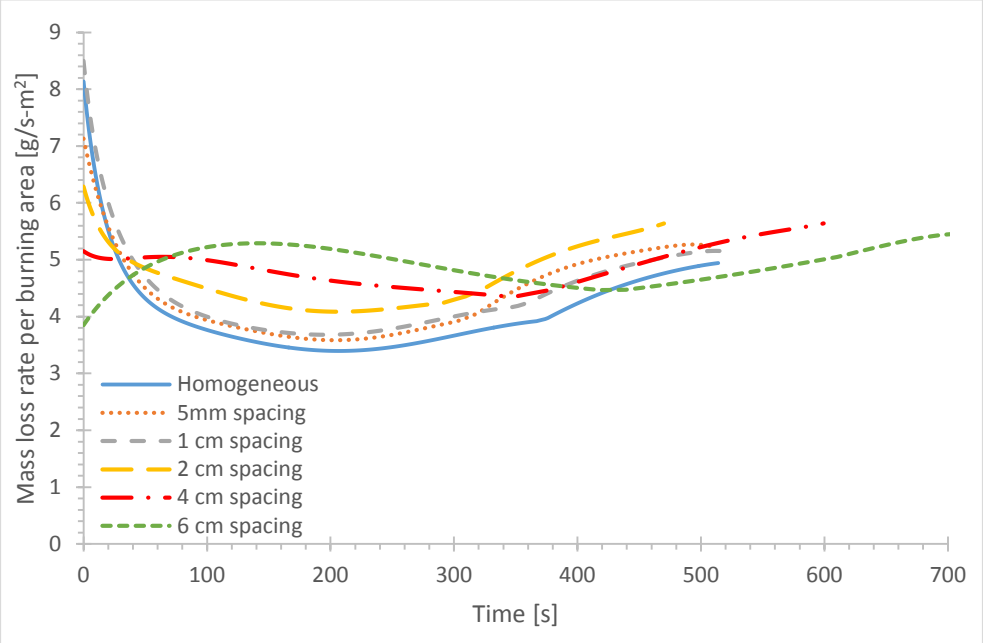

Figure 3.23. $\dot{m}"_{fuel}$ vs. time for the 4 cm fuel and homogeneous tests.

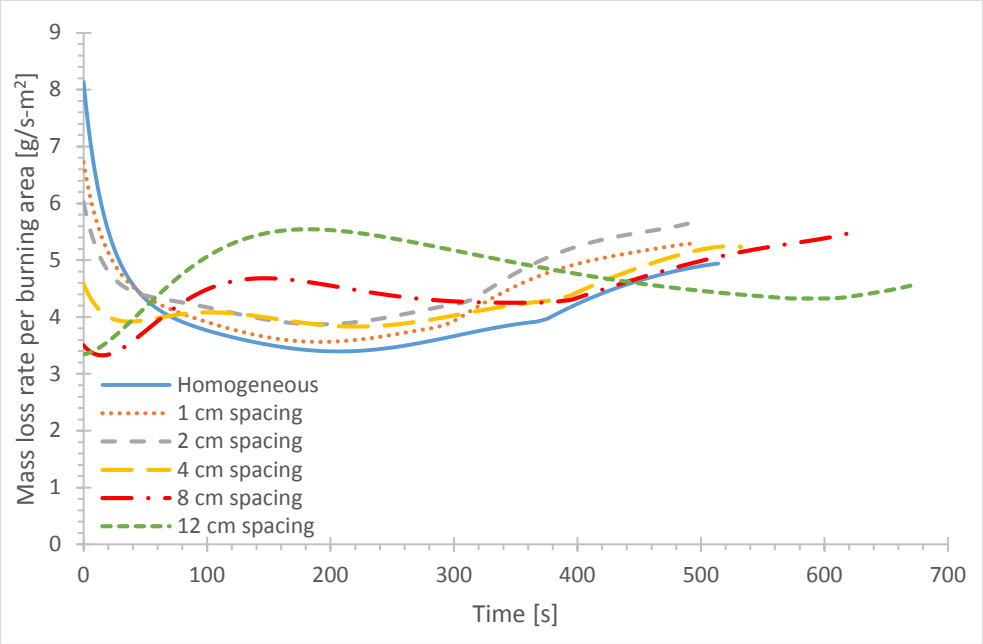

Figure 3.24. $\dot{m}''_{fuel}$ vs. time for the 8 cm fuel and homogeneous tests.

Other experimentalists have also examined mass loss rates per unit area for the homogeneous case. Gollner et al. obtained a value of 4 g/m²s for a spreading mass loss rate and 6 g/m²s for a steady mass loss rate in experimental work on 10 x 20 cm vertical PMMA slabs [24]. Experimental results from our research indicate a value of 3.5 – 4 g/m²s for the spreading phase and nearly 5 g/m²s towards the latter end of the data collection period. Considering this period was terminated before a maximum mass flux could be obtained, our results agree very well with Gollner et al.'s. Some researchers have recorded higher steady mass fluxes for PMMA, notably Ohtani et al. with 8 g/m²s, Singh et al. with 8.90 g/m²s, and Kulkarni et al. with with 9 g/m²s [48 - 50]. Regardless, these values were obtained with laminar flames across samples of significantly smaller size, so the higher mass loss rates are not surprising.

3.6 Limits of Flame Spread

All test data within this research project was extracted from experiments where the pyrolysis front successfully propagated over the entire fuel array. Nevertheless, there are certain configurations of fuel in which the height of the insulation will be too great for the flame to successfully spread over the whole apparatus. These limits were briefly investigated. An array with 4 cm blocks of fuel and 8 cm blocks of insulation was tested, and this experimental setup possessed a fuel percentage of 33%. The flame spread over the lower half of the apparatus, but it failed to reach the top of this fuel array before burnout of the already ignited portions began to occur, so the flame was extinguished. Further analysis with the IR camera revealed that the unignited portion of this test had actually just reached the ignition temperature criterion of 300^{o}C. If burnout of the lower regions of fuel did not occur, it is plausible that the pyrolysis front may have propagated across the whole of the apparatus. Extensive testing of the limits for 4 cm fuel arrays was not performed; nevertheless, these results certainly indicate that the limit of flame spread for 4 cm fuel lies somewhere just below a fuel percentage of 33%.

Chapter 4: Analysis

4.1 Flame Spread Rate

The general trend for flame spread to peak at an optimum fuel percentage indicates that entrainment may play a significant role in the flame spread rate. For the fastest flame spread case, a favorable fuel-to-oxidizer ratio may be provided by the gaps in the discretized fuel. These gaps may increase the amount of air entrained from both the front and the sides of the fuel array, so that the most efficient mixing would occur at an optimal fuel percentage. An increase or decrease in this optimal fuel percentage will reduce the flame spread. The 'optimal' configuration is a loose term, and it will change depending on the size and nature of the fuel utilized. For example, the addition of sidewalls could hypothetically reduce the amount of side entrainment, which could shift the optimal fuel percentage. A narrower fuel array could increase the influence of entrainment from the sides. The optimal configuration for a dissimilar fuel choice may occur at a different fuel percentage. Nevertheless, an optimal entrainment configuration will be defined as that which leads to the highest flame spread rate for the 20-cm-wide PMMA in this experimental setup.

The trend for this optimal configuration to occur at a specific fuel percentage is similar to the findings of Rothermel, who found an optimal packing density for porous fuels [34]. Watanabe et al. also found that filter paper with 20-30% porosity exhibited the fastest flame spread rate [37]. Both of these studies, although they tested significantly different experimental scenarios, found optimal configurations for the flame spread rate.

Returning to the thermal model of flame spread, we can surmise that the flame spread rate is directly related to both the magnitude and location of the heat flux directed to unburnt fuel. Continuing along this path of deduction, one can then hypothesize that an optimal entrainment configuration exhibits a heat flux profile that promotes involvement of fuel at further upward locations. This configuration is likely a multi-faceted function, dependent on flame characteristics, flame height, fuel location, fuel properties, etc. Regardless, our research clearly indicates that the fuel percentage of the array is a significant player in the flame spread rate. An understanding of the optimal fuel percentage for flame spread can help to quantify and compare the dangers of flame spread over discrete fuel loads. The ability for fire to propagate faster over discrete fuels with spacing is one very important extrapolation from these results. This implies that a disjoint scattering of fuel may actually pose a greater hazard than a dense, consolidated fuel distribution.

Figure 4.1 plots flame spread and fuel spread velocities for the 4 cm fuel and homogeneous tests. The optimal configuration can be easily identified as the fuel percentage of 67%, where a flame spread rate, V_p, of 0.091 cm/s occurs. This peak in the flame spread rate, at a fuel percentage of 67%, implies that this distribution of fuel represents a significant fire hazard. Meanwhile, the fuel spread velocity, $V_{p,fuel}$, exhibits a clear positive correlation with the fuel percentage, with a maximum value of 0.080 cm/s occurring in the homogeneous case. This correlation implies that fires in a homogeneous case, although they will not spread fastest, will more quickly involve greater quantities of fuel.

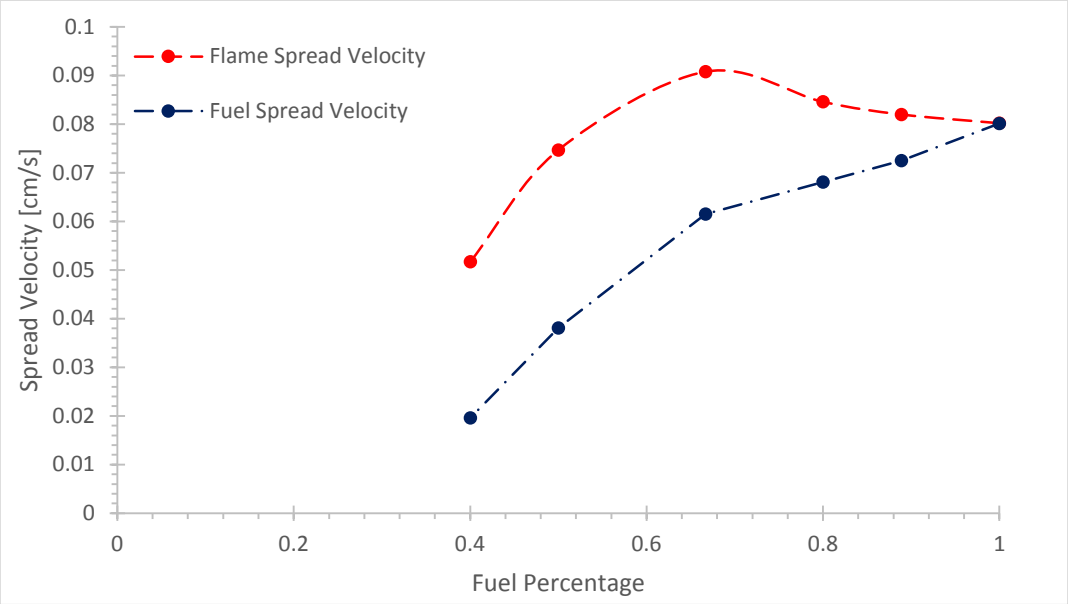

Figure 4.1. Flame spread and fuel spread velocities vs. fuel percentage for the 4 cm fuel and homogeneous tests.

Figure 4.2 plots flame spread and fuel spread velocities for the 8 cm fuel and homogeneous tests. In these results, the greatest flame spread rate, V_p, occurs at fuel percentages of 67%, 80%, and 89%, all of which exhibit flame spread rates of 0.09 cm/s. The optimal configuration, consequently, must lie somewhere within this region; fuel percentages outside of this region exhibit lower flame spread rates. On the other hand, the fuel spread velocity, $V_{p,fuel}$, is positively correlated to the fuel percentage. When plotted vs. fuel percentage, these results for spread rates are very similar to those for the 4 cm and homogeneous tests.

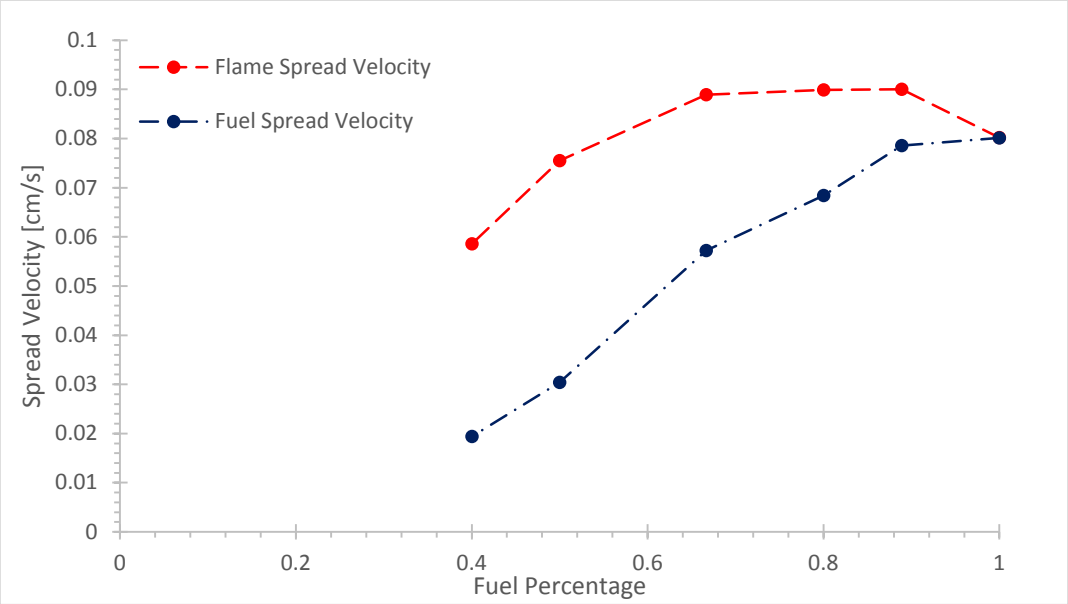

Figure 4.2. Flame spread and fuel spread velocities vs. fuel percentage for the 8 cm fuel and homogeneous tests.

When the fuel percentage is the result of a uniform distribution of discrete fuels, knowledge of either the flame spread rate or the fuel spread rate also allows us to predict the other. For instance, Equation 4.1 was used to predict the flame spread rate from the fuel spread rate:

$$V_p = \frac{V_{p,fuel}}{(fuel\ \%)} \tag{4.1}$$

The resulting estimates for the flame spread rate are plotted in Figures 4.3 and 4.4, and they lie in relative agreement with the experimental results. Equation 4.1 could also be used to estimate the fuel spread rate from the flame spread rate. This technique would likely fall apart if a given fuel array experienced dramatic fluctuations in the important length scales (i.e., fuel and spacing lengths).

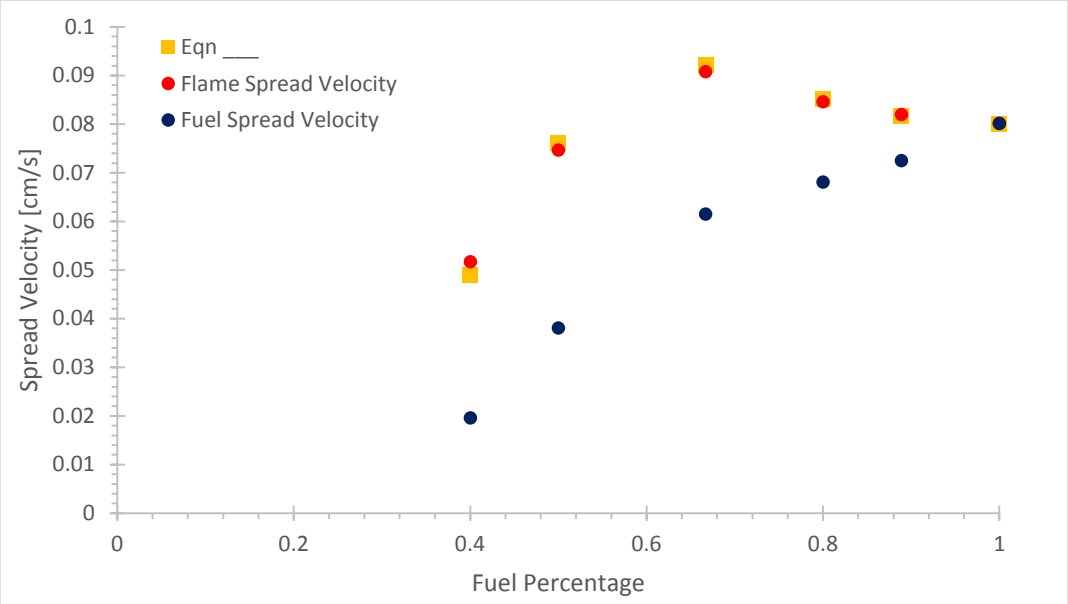

Figure 4.3. Flame spread velocities, fuel spread velocities, and estimates for the flame spread velocities derived from fuel spread velocities via equation 4.1. Data shown is from 4 cm fuel and homogeneous tests.

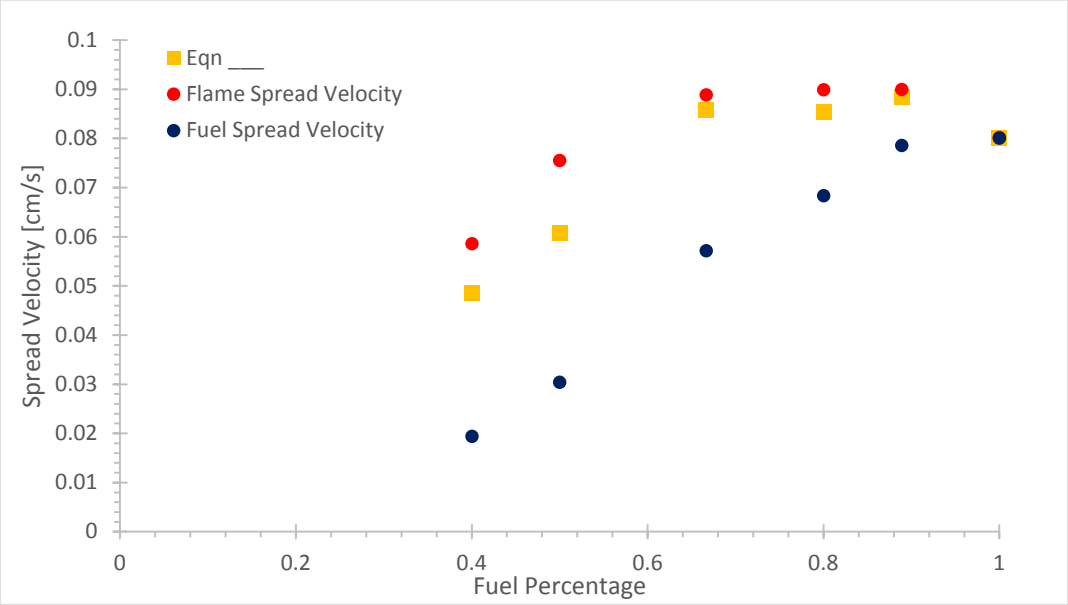

Figure 4.4. Flame spread velocities, fuel spread velocities, and estimates for the flame spread velocities derived from fuel spread velocities via equation 4.1. Data shown is from 8 cm fuel and homogeneous tests.

The fuel spread velocity exhibits a trend that could be estimated if the limits of the fuel spread rate are known. The homogeneous fuel spread velocity can be measured experimentally; additionally, our experiments with discrete fuels tend to exhibit a limit where no spread occurs somewhere around a fuel percentage of 30%. By measuring the homogeneous spread and assuming a fuel spread velocity of zero at a certain critical fuel percentage, $(fuel\,\%)_{crit}$, a logarithmic fit can be applied to these two points to create an estimate of the fuel spread rate. The logarithmic fit would then take the form

$$V_{p,fuel} = a\ln(x) + b, \tag{4.2}$$

where $b = V_{p,homogeneous} = V_{p,fuel,homogeneous}$, x represents the fuel percentage, and $a = \frac{-b}{\ln[(fuel\,\%)_{crit}]}$. Given this estimation for the fuel spread velocity, V_p could then be estimated by means of Equation 4.1.

This methodology was applied to the spread rates that were obtained, and the following values were employed:

$$V_{p,homogeneous} = 0.08\ cm/s$$

$$(fuel\,\%)_{crit} = 0.27$$

Here, the homogeneous spread rate was derived from experimental results and the critical fuel percentage was estimated based on results for tests with low fuel percentage. The following constants were then obtained:

$$b = V_{p,homogeneous} = 0.08$$

$$a = \frac{-b}{\ln[(fuel\,\%)_{crit}]} = \frac{-0.08}{\ln(0.27)} = 0.061$$

Plugging these results into Equation 4.2, we have

$$V_{p,fuel} = 0.061 \ln(x) + 0.08, \tag{4.3}$$

where x is the fuel percentage. Figure 4.5 plots this theoretical fit vs. experimental results from all tests; the theory fits the results well, revealing an R^2-value of 0.97. Moving further, the results from the theoretical fit for fuel spread rate can be used to estimate flame spread rates via Equation 4.1. These hypothetical flame spread rates are also plotted vs. experimental results in Figure 4.5. This fit attains an R^2-value of 0.84.

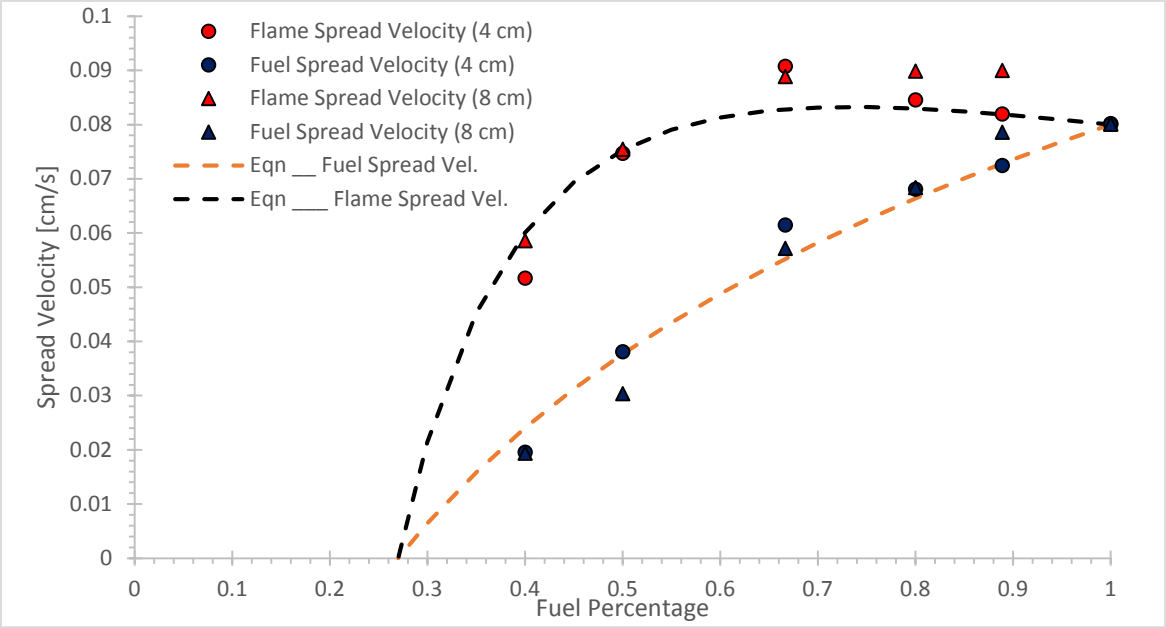

Figure 4.5. Plot of the spread velocities from all tests and estimates from Equations 4.3 and 4.1 vs. fuel percentage.

Overall, the theoretical results from estimation of the limits of flame spread fits the data remarkably well. The fit for the fuel spread velocity is quite adequate, reaffirming our hypothesis that no spread will occur around a limiting fuel percentage of 27%. The positive correlation of fuel spread velocity with fuel percentage is perhaps the most consistent trend in this study, and

a logarithmic fit captures the expected behavior well. The fit for the flame spread velocity is reasonable as well; only slight underpredictions are observed for the higher fuel percentages.

It should also be noted that results for the 4 and 8 cm fuel arrays with identical fuel percentages are quite comparable. Moreover, the trends observed for the flame spread and fuel spread rates are the same. For fuels in the small range of tested sizes, it appears that relevant relationships for flame spread scale with the fuel percentage. It is not clear whether this trend would continue scale beyond fuels in the 4-8 cm range; unfortunately, the small size of the apparatus and the lack of precision needed for smaller fuel blocks made testing of other fuel sizes beyond the realm of this study.

4.2 Acceleration of Spread Rate

The aforementioned values for the flame spread velocity have been derived from an average data sample across the distance 10 to 25 cm from the bottom of the fuel array. However, the rate of flame spread is not a static variable for upward flame spread, and many experiments with samples of necessary height have observed significant acceleration of the flame spread rate [30]. Our experiment is no exception. By dividing the height of the fuel array into five separate regions, we were able to look at velocities observed at various locations. A linear fit was applied to the data in each region (i.e. measurement locations and ignition times) to estimate local flame spread rates.

Figure 4.6 displays a plots of the local flame spread velocity vs. location for the 4 cm fuel and homogeneous cases. For the arrays with a fuel percentage of 80% and higher, a clear

acceleration can be identified as the pyrolysis front advances up the apparatus. Meanwhile, the test with 2 cm spacing exhibits an unclear trend, although the velocity magnitude of the uppermost region seems to indicate that some acceleratory effects are certainly possible. However, the local flame spread rates of the remaining tests, involving 4 and 6 cm spacings, seem to indicate a deceleration of the pyrolysis front. It seems that the low fuel percentage begins to have a significant impact in the later stages of flame spread. The decreased flame height may have a large effect at higher regions, where radiative effects become more pronounced and the heat transfer is no longer dominated by a laminar flame. Additional experimentation on a larger apparatus may even indicate that the upward flame spread for tests with lower fuel percentages may further decelerate or even fail to propagate at higher regions.

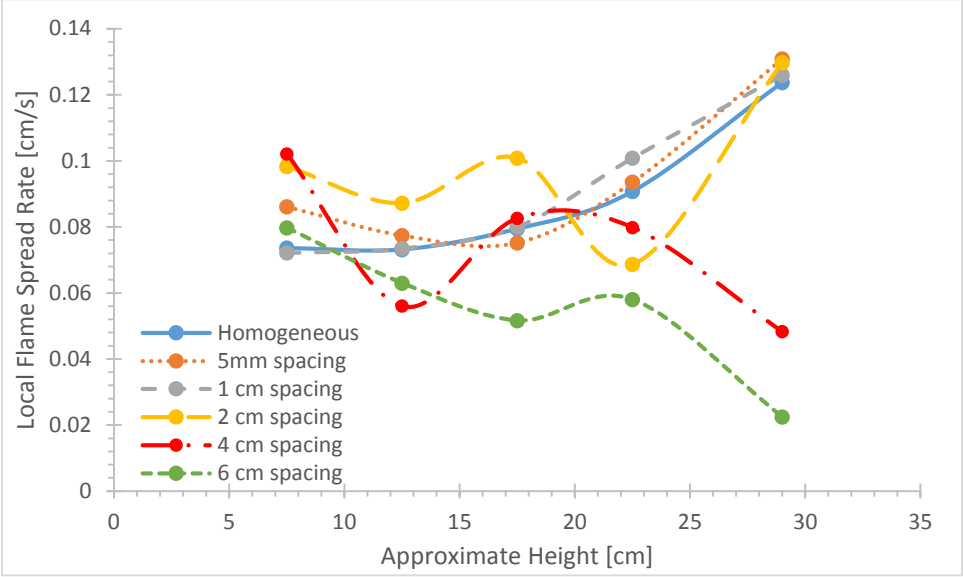

Figure 4.6. Local flame spread rates vs. height for the 4 cm fuel and homogeneous tests.

Figure 4.7 displays a plots of the local flame spread velocity vs. location for the 8 cm fuel and homogeneous cases. Similar to the 4 cm fuel arrays, the 8 cm fuel tests with a high fuel percentage seem to exhibit at least some acceleratory effects; this is evidenced by the larger local

flame spread rates at higher regions of the apparatus. Meanwhile, the 8 cm fuel tests with lower fuel percentages (i.e., arrays with 8 and 12 cm spacings) have clearly decelerated towards the top of the apparatus. These findings parallel the trends observed in the 4 cm fuel arrays.

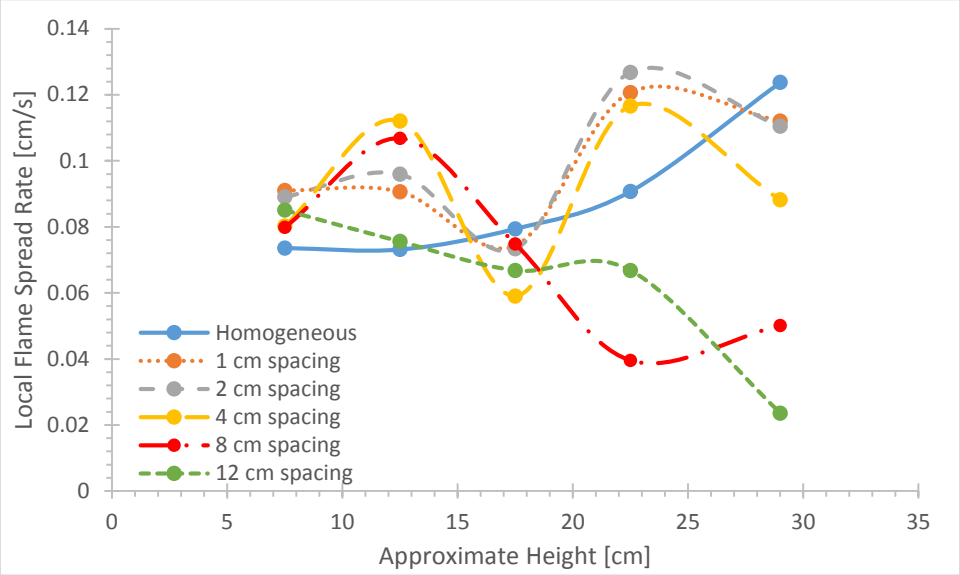

Figure 4.7. Local flame spread rates vs. height for the 8 cm fuel and homogeneous tests.

These plots display a sharp divergence in acceleratory trends of the pyrolysis front for arrays with a low fuel percentage vs. arrays with a high fuel percentage. These results indicate that different flame spread behaviors are occurring. A flame front for all discrete fuels spreads via a 'jumping' phenomenon, whereby the pyrolysis front will ascend to the top of one block of fuel and momentarily halt. After a certain amount of time, the next block of fuel will be heated to the point where the pyrolysis front can effectively 'jump' to this block of fuel and resume its progress. Because it takes a significant amount of time for this jump to occur at low fuel percentages, the flame propagates in a very iterative fashion. Because each successive iteration (i.e., jump from one fuel to the next), appears to take a greater amount of time, an eventual failure to spread on a larger apparatus is a plausible. On the other hand, the flame spread behavior for

high fuel percentages is indicative of a flame that is continuously advancing. This divergence in behavior indicates that there is a certain fuel percentage below which fuel arrays should be treated as distinctly discrete. Above this fuel percentage, the flame spread may actually be described as a partially homogeneous fuel bed.

4.3 Shape of Pyrolysis Front

Although flame spread rates were calculated by only looking at 2-cm wide line measurements along the centerline, the infrared images also provide information about the temperature profiles along the entire width of the apparatus. Consequently, IR images can quickly provide qualitative information about the location and shape of the pyrolysis front. These images were examined to determine whether any anomalies in the development of the pyrolysis front occurred between any tests. No abnormalities or strange trends were readily detectable as the pyrolysis front seemed to attain the same U-shape under all testing conditions. Figure 4.8 provides a series of IR images that display the approximate shape of the pyrolysis front at the height of the homogeneous and 4 cm fuel arrays. All tests held roughly the same shape of the pyrolysis front, the only real differences being slight outward bulges along the inert regions, which do not represent the true pyrolysis region anyhow.

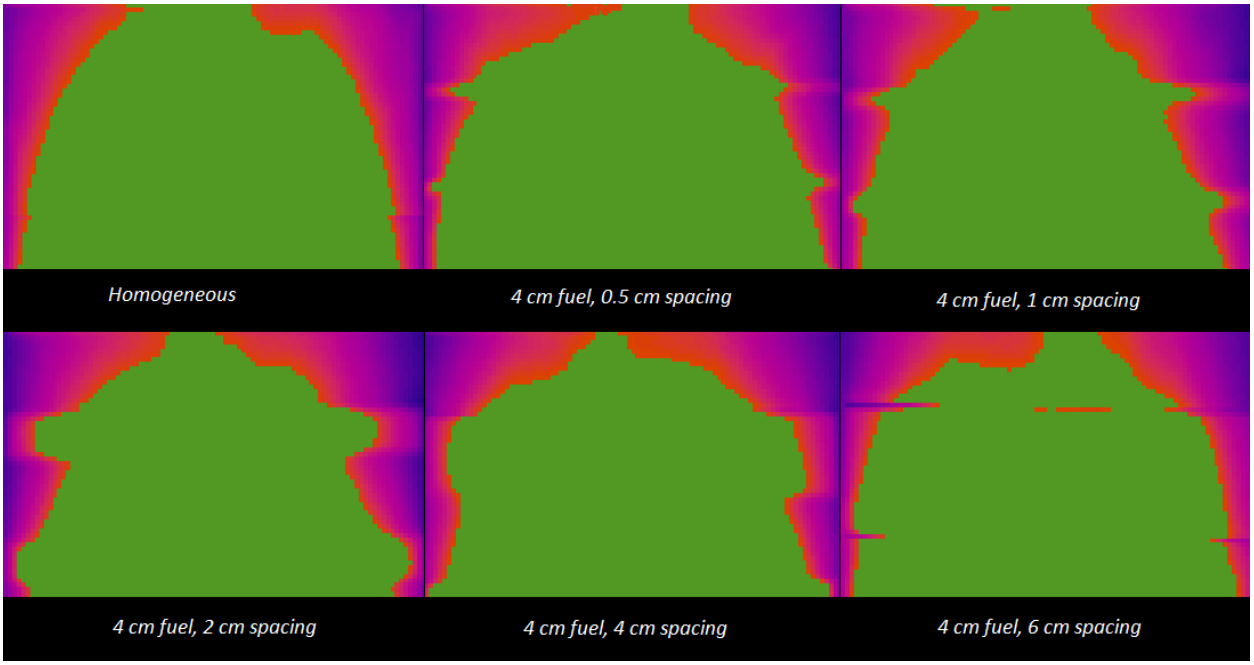

Figure 4.8. Illustration of the pyrolysis front shape upon reaching the top of the apparatus for several tests. The highlighted green portion of each picture represents temperature values above the pyrolysis temperature (i.e., greater than 300°C).

The U-shape of the pyrolysis front seems to indicate that there are slight edge effects, but these effects do not appear to detrimental. Moreover, these slight edge effects do not get amplified under any of the test conditions tested. The only concern warranted by the shape of the pyrolysis front is that the burning area, which is calculated from centerline measurements, is overestimated. This may lead to slight discrepancies in numerical results, but it should not significantly alter any of the trends observed among tested fuel arrays.

4.4 Mass Fluxes during Representative Spreading Phase

Average mass loss rates per unit area were estimated over the time period when the linear fit for $x_{p,total}$ occupied 10-25 cm in height. This region is the middle of the fuel array, and the

associated time period represents the middle portion of the flame spread phase. Both $\dot{m}"_{fuel}$ and $\dot{m}"_{total}$ were averaged over this period, and the results are plotted vs. fuel percentage in Figures 4.9 and 4.10. For all tests, $\dot{m}"_{total}$ is nearly constant during the spreading phase, hardly deviating from around 3 g/s-m^2. However, $\dot{m}"_{fuel}$ appears to be negatively correlated with fuel percentage. The highest results for $\dot{m}"_{fuel}$ actually occur for the tests with the lowest fuel percentage, climbing to over 5 g/s-m^2.

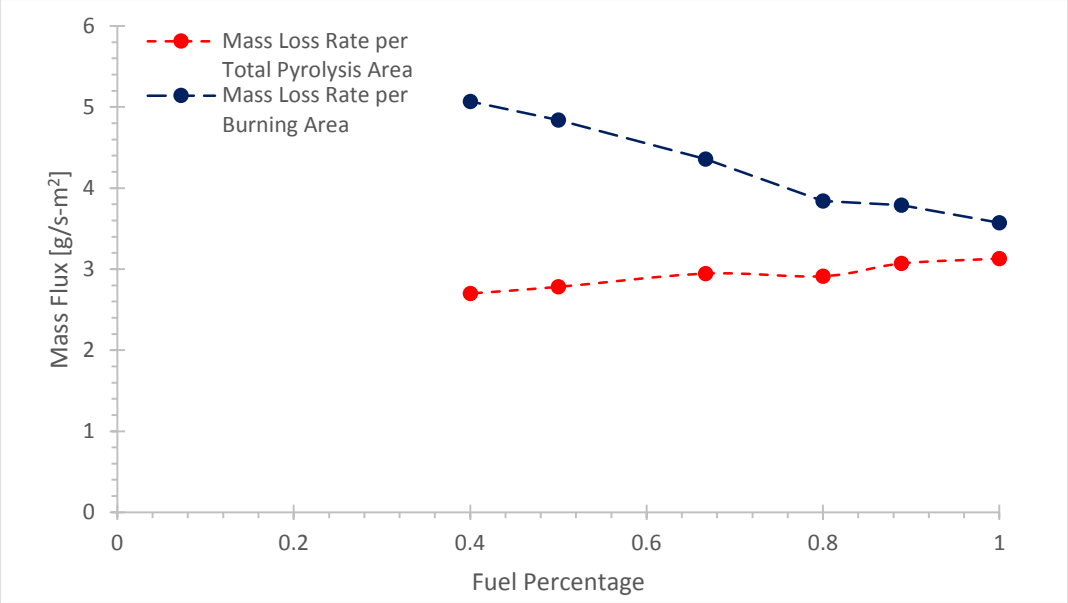

Figure 4.9. Averages for $\dot{m}"_{fuel}$ and $\dot{m}"_{total}$ during the spreading phase vs. fuel percentage for the 4 cm fuel and homogeneous tests. Please note that the difference in the mass flux values for the homogeneous test is the result of the inclusion of the 2-cm-tall insulation above the ignition block for the total area calculations.

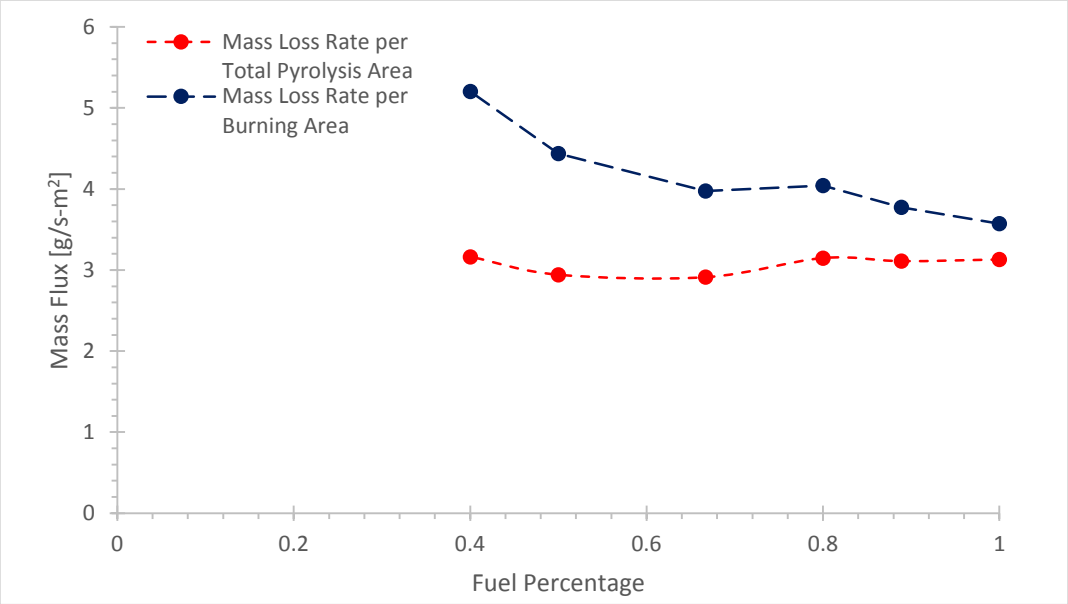

Figure 4.10. Averages for $\dot{m}''_{fuel}$ and $\dot{m}''_{total}$ during the spreading phase vs. fuel percentage for the 8 cm fuel and homogeneous tests.

These results imply that, during the spreading phase, the fuel from the arrays with more spacing are releasing more pyrolyzed gases per surface area of fuel. These results imply that a higher heat flux per unit area is being imparted over the fuel surface. This could be a result of a decreased flame standoff distance, which would allow a greater heat flux to be delivered to the fuel array. This could also be caused by greater air entrainment due to the spacings; perhaps the greater availability of fresh oxidizer is increasing the flame temperature. If this is true, it may help to elucidate a further mechanism contributing to a faster flame spread rate at a fuel percentage below unity. The higher local mass flux of gases at lower fuel percentages will assist the flame in overcoming the obstacles in spread provided by inert spacing. The mass flux data further supports the argument that the flame spread rate is dependent on the entrainment of fresh oxidizer.

One could argue that these results are skewed because they are derived from a linear fit for $x_{p,fuel}$. It is certainly true that the actual burning area does not follow a strictly linear growth, particularly in the low fuel percentage tests; in these tests, an iterative jumping phenomenon is observed as the pyrolysis front halts at the top of one block of fuel while the next block of fuel is slowly heated to its pyrolysis temperature. Regardless, the results for the mass fluxes should still hold because they have resulted from an average of results over a significant span of time. The discrepancies in the instantaneous calculation of the burning area should have only minor effects on the results displayed here because the linear fit for $x_{p,fuel}$ provides an adequate measure of the *average* burning region.

Furthermore, the shape of the pyrolysis front does not appear to deviate much between different fuel arrays. This qualitative assessment, which was made in the previous section, should assuage concerns that the predicted trend is a result of width differences in the actual burning region between tests. Although the exactness of the numerical values provided are debatable, it seems unlikely that the observed trends are systematic errors.

4.5 Comparison to a Relevant Flame Height Correlation

Multiple experimentalists have investigated correlations related to flame height; however, some correlations more readily apply to certain scenarios than others. Delichatsios hypothesized a simplified flame height correlation for turbulent wall fires on the basis of dimensional analysis, suggesting the flame height depends only on the fire heat release rate to the $^2/_3$ power [51]. Gollner et al. later investigated smaller, laminar wall fires where, via dimensional analysis, they

found a $^4/_3$ scaling relationship of the flame height with the fire heat release rate [15]. Experimental observations seem to agree with these scaling approaches. Larger experiments by others [52, 53] agree with the $^2/_3$ turbulent correlation while smaller scale studies, such as those presented here, often scale with unity [29]. A correlation performed by Tsai and Drysdale was recently submitted from a similar experiment, in which flame heights from a vertical sample of PMMA were investigated [29]. For the experiments involving an extended plate (similar to the setup here), it was found that the flame height was correlated with the heat release rate per unit width in the following relationship:

$$x_f = 0.011\dot{Q}'^{1.25} \quad for\ 10 \leq \dot{Q}' \leq 30 kW/m \tag{4.4}$$

where x_f is in meters and $\dot{Q}'$ is in kW/m. This correlation was plotted vs. results from the homogeneous and 4 cm fuel arrays and vs. data from the homogeneous and 8 cm arrays in Figures 4.11 and 4.12. These figures plot x_f vs. $\dot{Q}'$, where $\dot{Q}'$ was determined from the mass loss rate via the following equation:

$$\dot{Q}' = \frac{\dot{m}\Delta h_c}{w} \tag{4.5}$$

where Δh_c is the heat of combustion of PMMA (25 kJ/g) and w the width of the fuel array (0.2 m) [54].

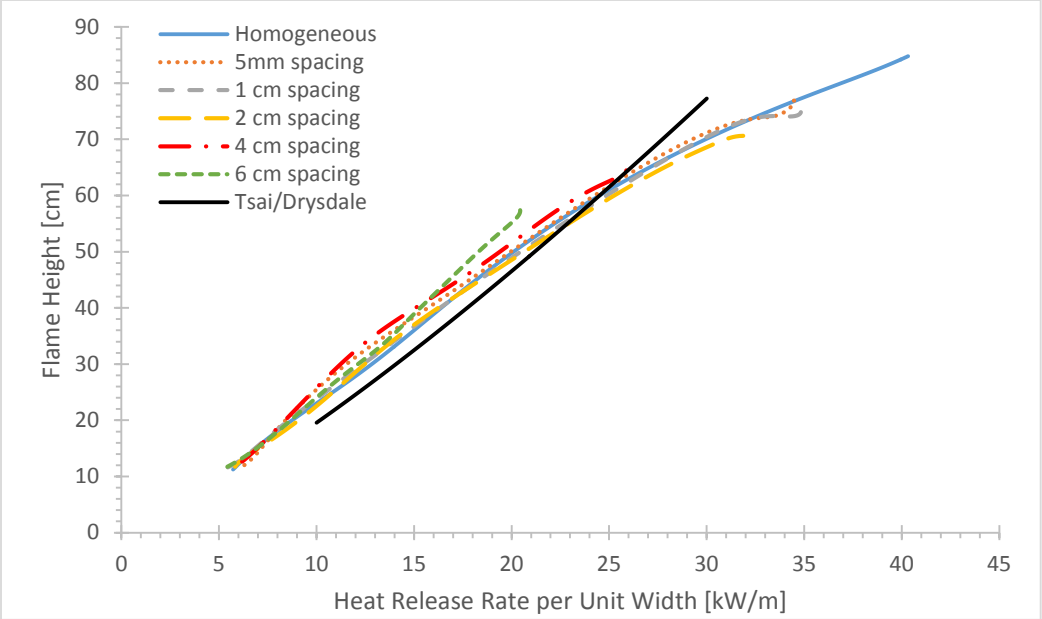

Figure 4.11. Flame heights vs. the heat release rate per unit width for the 4 cm fuel and homogeneous tests. The expected flame height from Tsai and Drysdale's most relevant correlation is also plotted.

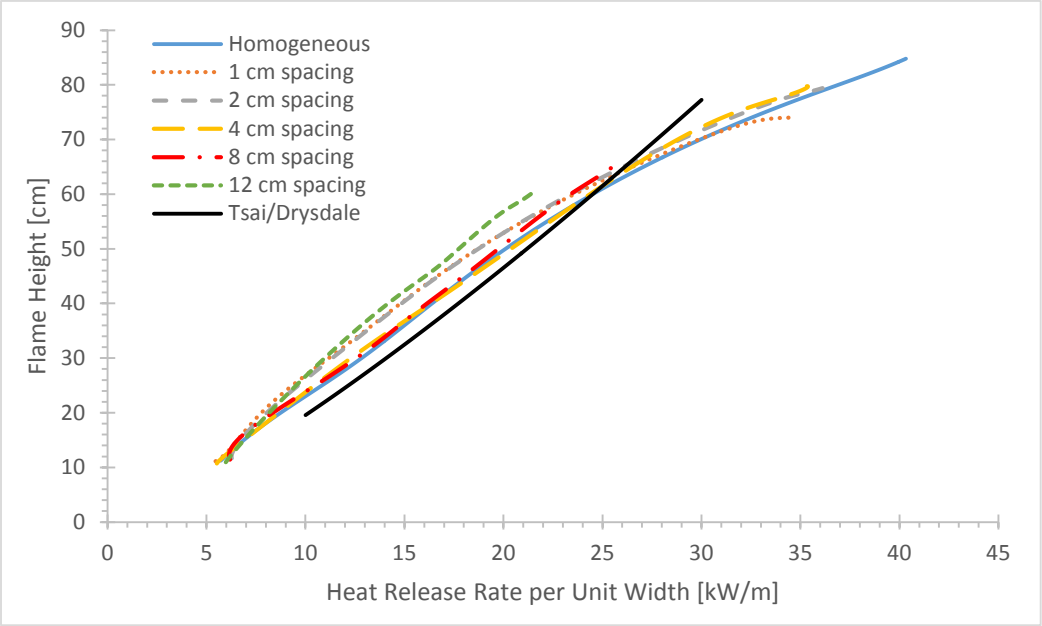

Figure 4.12. Flame heights vs. the heat release rate per unit width for the 8 cm fuel and homogeneous tests. The expected flame height from Tsai and Drysdale's most relevant correlation is also plotted.

The correlation from Tsai and Drysdale estimates a flame height that is comparable to observed flame heights for all tests. As a point of comparison, a power law fit was also applied to the average of the homogeneous fuel results, and the following correlation was developed with an R^2-value of 0.99:

$$x_{f,homogeneous} \approx 0.021\dot{Q}'^{1.05} \quad for\ 10 \leq \dot{Q}' \leq 30kW/m \tag{4.6}$$

The exponential power of this fit is slightly less than Tsai and Drysdale. Power law fits were also briefly assessed for all tests in the range of $5 \leq \dot{Q}' \leq 20kW/m$, and it was found that, for all fits of the form $x_f \sim \dot{Q}'^{\eta}$, η lied between the values 1.11 and 1.23.

Figures 4.11 and 4.12 confirm that the flame height is positively correlated with $\dot{Q}'$, and consequently the mass loss rate as well, across all tests. A closer look at these figures reveals that the tests with the lowest fuel percentage had slightly higher flame heights for the range $15 \leq \dot{Q}' \leq 20kW/m$. This indicates that the low fuel percentage may have resulted in the distribution of the mass flux across a greater length of the apparatus, causing a slightly taller flame at these mass fluxes.

Chapter 5: Conclusion

This study has analyzed upward flame spread over discrete fuels by studying vertical arrays of alternating lengths of PMMA and insulation. By manipulating the lengths of the fuel and insulation, various results were generated and several important trends related to flame spread were assessed.

Perhaps the most noteworthy finding is the trend for the flame spread rate to peak at a fuel percentage below unity. For the 4 cm fuel, a peak flame spread rate occurred at a fuel percentage of 67%; for the 8 cm fuel, a peak flame spread rate was shared by fuel percentages 67%, 80%, and 89%. It has been hypothesized that these fuel percentages witness a larger flame spread rate than the homogeneous case because of the increased air entrainment. If extrapolation of these results is possible, the implication would be that fuel loads with greater spacing between discrete fuels could represent a greater fire hazard than a concentrated distribution of fuel.

It was discovered that the fuel spread rate follows a readily identifiable trend, which consists of a positive correlation with fuel percentage. Moreover, this study revealed that a reliable estimation of the fuel spread rate for various fuel percentages can be developed with knowledge of the homogeneous fuel spread rate and a reasonable assessment for the limiting fuel percentage. In turn, the flame spread rate can be approximated for a given fuel array if the fuel spread rate is known. This methodology may serve as a useful foundation for estimates of flame spread rates without extensive testing.

The mass loss rate per burning area was found to be negatively correlated with fuel percentage. These results imply that a higher heat flux is being imparted over the fuel surface.

The increased mass flux at low fuel percentages likely contributes to the aforementioned trend for the flame spread rate.

A flame front for discrete fuels spreads via a 'jumping' phenomenon, whereby the pyrolysis front will ascend to the top of one block of fuel and momentarily halt. After a certain amount of time, the next block of fuel would be heated to the point where the pyrolysis front can effectively 'jump' to this block of fuel and resume its progress. For low fuel percentages, it was discovered that the time for the pyrolysis front to jump to the next block of fuel could be significant. Furthermore, the lower fuel percentages witnessed a deceleration of the pyrolysis front after each successive jumping iteration. Higher fuel percentages still exhibited the expected acceleration of the pyrolysis front as it moves upward. This divergence of behavior indicates that the conditions in the more developed stages of upward flame spread may lead to different results. Additionally, the divergence of results indicates that there is a fuel percentage below which an assumption of near-homogeneity is invalid; consequently, the fuel configuration should be identified as distinctly discrete.

Further research would assist the validation of these hypotheses. Recommendations for subsequent studies include: the addition of sidewalls to determine the influence of lateral diffusion; increased length scales for fuels and apparatuses; testing of varying fuels; and forced flow, horizontal configurations.

This study has identified several empirical trends for upward flame spread over discrete fuels. These trends elucidate important variables that play a role in the observed phenomenon. An understanding of these behaviors is vital to predicting and quantifying this important fire scenario.

References

[1] Karter, M. (2013, September). Fire loss in the United States. Retrieved from http://www.nfpa.org/research/reports-and-statistics/fires-in-the-us/overall-fire-problem/fire-loss-in-the-united-states

[2] Ito, A., & Kashiwagi, T. (February 01, 1988). Characterization of flame spread over PMMA using holographic interferometry sample orientation effects. *Combustion and Flame, 71*, 2, 189-204.

[3] National Fire Protection Association., & National Fire Protection Association. (2008).*NFPA 921, guide for fire and explosion investigations*. Quincy, Mass: National Fire Protection Association.

[4] Finney, M. A., Cohen, J. D., McAllister, S. S., & Jolly, W. M. (February 15, 2013). On the need for a theory of wildland fire spread. *International Journal of Wildland Fire, 22,* 1, 25-36.

[5] Grant, G. (January 01, 1995). Numerical modelling of early flame spread in warehouse fires. *Fire Safety Journal, 24,* 3, 247-278.

[6] Fernandez-Pello, A. C. (January 01, 1978). A theoretical model for the upward laminar spread of flames over vertical fuel surfaces. *Combustion and Flame, 31,* 135-148.

[7] Orloff, L,. Modak, A. T., & Alpert, R. L. *Sixteenth Symposium (International) on Combustion*, Combustion Institute, Pittsburgh, PA, 1976, pp. 1345-1354.

[8] Drysdale, D. D., & Macmillan, A. J. R. (January 01, 1992). Flame spread on inclined surfaces. *Fire Safety Journal, 18,* 3, 245-254

[9] Pizzo, Y., Consalvi, J. L., & Porterie, B. (January 01, 2009). A transient pyrolysis model based on the B-number for gravity-assisted flame spread over thick PMMA slabs.*Combustion and Flame, 156,* 9, 1856-1859.

[10] Orloff L., de Ris J., Markstein GH. Upward Turbulent Fire Spread and Burning of Fuel Surface. *15th Symposium (int.) on Combustion*, The Combustion Institute, 1974. p. 183-92.

[11] Saito, K., Quintiere, J. G., Williams F. A. Upward Turbulent Flame Spread. *Fire Saf Sci; Proceedings of the First International Symposium*, 1985, p. 75-86.

[12] Tewarson, A., & Ogden, S. D. (January 01, 1992). Fire behavior of polymethylmethacrylate. *Combustion and Flame, 89,* 3, 237-259.

[13] Fernandez-Pello, A. C. (January 01, 1978). A theoretical model for the upward laminar spread of flames over vertical fuel surfaces. *Combustion and Flame, 31,* 135-148.

[14] Audouin, L., Kolb, G., Torero, J. L., & Most, J. M. (January 01, 1995). Average centreline temperatures of a buoyant pool fire obtained by image processing of video recordings.*Fire Safety Journal, 24,* 2, 167-187.

[15] Gollner, M. J., Williams, F. A., & Rangwala, A. S. (January 01, 2011). Upward flame spread over corrugated cardboard. *Combustion and Flame, 158,* 7, 1404-1412.

[16] Rangwala, A. S., Buckley, S. G., & Torero, J. L. (January 01, 2007). Upward flame spread on a vertically oriented fuel surface: The effect of finite width. *Proceedings of the Combustion Institute, 31,* 2, 2607-2615.

[17] Consalvi, J. L., Pizzo, Y., Porterie, B., & Torero, J. L. (January 01, 2007). On the flame height definition for upward flame spread. *Fire Safety Journal, 42,* 5, 384-392.

[18] Quintiere, J., Harkelroad, M., & Hasemi, Y. (July 20, 1986). Wall Flames and Implications for Upward Flame Spread. *Combustion Science and Technology, 48,* 191-222.
[19] De, R. J. N. (January 01, 1969). Spread of a laminar diffusion flame. *Symposium (international) on Combustion, 12,* 1, 241-252.
[20] Williams, F. (January 01, 1977). Mechanisms of fire spread. *Symposium (international) on Combustion, 16,* 1, 1281-1294.
[21] Saito, K., Williams, F. A., Wichman, I. S., & Quintiere, J. G. (January 01, 1989). Upward Turbulent Flame Spread on Wood Under External Radiation. *Journal of Heat Transfer,111,* 2, 438
[22] Saito, K., Quintiere, J. G., Williams, F. A. *Fire Safety Science – Proc. First Inl. Symp* 1985, 75 – 86.
[23] Drysdale, D. D., & Macmillan, A. J. R. (January 01, 1992). Flame spread on inclined surfaces. *Fire Safety Journal, 18,* 3, 245-254.
[24] Gollner, M. J., Huang, X., Cobian, J., Rangwala, A. S., & Williams, F. A. (January 01, 2013). Experimental study of upward flame spread of an inclined fuel surface.*Proceedings of the Combustion Institute, 34,* 2, 2531-2538.
[25] Rangwala, A. S., Buckley, S. G., & Torero, J. L. (January 01, 2007). Upward flame spread on a vertically oriented fuel surface: The effect of finite width. *Proceedings of the Combustion Institute, 31,* 2, 2607-2615.
[26] Tsai, K., & Wan, F. (January 01, 2005). Upward Flame Spread: The Width Effect. *Fire Safety Science, 8,* 409-419.
[27] Pizzo, Y., Consalvi, J. L., Querre, P., Coutin, M., & Porterie, B. (April 01, 2009). Width effects on the early stage of upward flame spread over PMMA slabs: Experimental observations. *Fire Safety Journal, 44,* 3, 407-414.
[28] Tsai, K.-C. (January 01, 2011). Influence of sidewalls on width effects of upward flame spread. *Fire Safety Journal, 46,* 5, 294-304.
[29] Tsai, K.-C., & Drysdale, D. (November 01, 2002). Flame height correlation and upward flame spread modelling. *Fire and Materials, 26,* 6, 279-287.
[30] Qian, C., & Saito, K. (January 01, 1997). An Empirical Model For Upward Flame Spread Over Vertical Flat And Corner Walls. *Fire Safety Science, 5,* 285-296.
[31] Thomas, P. H. (January 01, 1971). Rates of Spread of Some Wind-driven Fires.*Forestry, 44,* 2, 155-175.
[32] Thomas, P. H. (January 01, 1967). Some Aspects of the Growth and Spread of Fire in the Open. *Forestry, 40,* 2, 139-164.
[33] Dupuy, J. L. (January 01, 1995). Slope and Fuel Load Effects on Fire Behavior: Laboratory Experiments in Pine Needles Fuel Beds. *International Journal of Wildland Fire,5,* 3.)
[34] Rothermel, R. C., Intermountain Forest and Range Experiment Station (Ogden, Utah),, & United States. (1972). *A mathematical model for predicting fire spread in wildland fuels.*
[35] Emmons, H. W., & Shen, T. (January 01, 1971). Fire spread in paper arrays. *Symposium (international) on Combustion, 13,* 1, 917-926.
[36] Finney, M. A., Cohen, J. D., Grenfell, I. C., & Yedinak, K. M. (April 16, 2010). An examination of fire spread thresholds in discontinuous fuel beds. *International Journal of Wildland Fire, 19,* 2, 163-170.

[37] Watanabe, Y., Torikai, H., & Ito, A. (January 01, 2011). Flame spread along a thin solid randomly distributed combustible and noncombustible areas. *Proceedings of the Combustion Institute, 33*, 2, 2449-2455.
[38] Abe, S., Ito, A., & Torikai, H. (September 01, 2012). Flame spread along a thin combustible solid with randomly distributed square pores of two different sizes. *Modern Applied Science, 6*, 9, 11-19.
[39] Vogel, M., & Williams, F. A. (May 01, 1970). Flame Propagation Along Matchstick Arrays. *Combustion Science and Technology, 1*, 6, 429-436.
[40] Prahl, J., & Tien, J. (August 01, 1973). Preliminary Investigations of Forced Convection on Flame Propagation along Paper and Matchstick Arrays. *Combustion Science and Technology, 7*, 6, 271-282.
[41] WOLFF, M. F., CARRIER, G. F., & FENDELL, F. E. (June 01, 1991). Wind-Aided Firespread Across Arrays of Discrete Fuel Elements. I. Theory. *Combustion Science and Technology, 77*, 261-289.
[42] Hwang, C. C., & Xie, Y. (1984). Flame Propagation Along Matchstick Arrays On Inclined Base Boards. *Combustion Science and Technology, 41, 1-2*.
[43] Gollner, M. J., Xie, Y., Lee, M., Nakamura, Y., & Rangwala, A. S. (May 01, 2012). Burning Behavior of Vertical Matchstick Arrays. *Combustion Science and Technology, 184*, 5, 585-607.
[44] Kashiwagi, T., Inaba, A. and Brown, J.E., (1986). Differences In Pmma Degradation Characteristics And Their Effects On Its Fire Properties. *Fire Safety Science 1*: 483-493.
[45] Melendez, J., Foronda, A., Aranda, J. M., Lopez, F., & del, C. F. J. L. (January 01, 2010). Infrared thermography of solid surfaces in a fire. *Measurement Science & Technology, 21*, 10, 105504.
[46] Urbas, J., Parker, W. J., & Luebbers, G. E. (January 01, 2004). Surface temperature measurements on burning materials using an infrared pyrometer: accounting for emissivity and reflection of external radiation. *Fire and Materials, 28*, 1, 33-53.
[47] Sohn, Y., Seung, W. B., & Kashiwagi, T. (January 01, 1999). Transient Modeling of Thermal Degradation in Non-Charring Solids. *Combustion Science and Technology New York Then Yverdon-, 145*, 83-108.
[48] Ohtani, H., Ohta, K., & Uehara, Y. (October 01, 1991). Effect of orientation on burning rate of solid combustible. *Fire and Materials, 15*, 4, 191-193.
[49] Singh, A. V., & Gollner, M. J. (June 01, 2014). Estimation of local mass burning rates for steady laminar boundary layer diffusion flames. *Proceedings of the Combustion Institute,*4.)
[50] Kulkarni, A. K., Kim, C. I., & Mitler, H. E. (1991) Time-dependent Local Mass Loss Rate of Finite-thickness Burning Walls of PMMA. *Heat and Mass Transfer in Fires and Combustion Systems*. HTD-Vol. 176.
[51] Delichatsios, M. A. (1984) *Combust. Sci. Technol.* 39: 195-214.
[52] Quintiere, J. G., Harkleroad, M., & Hasemi, Y. *Combust. Sci. Technol. 48*: 191-222.
[53] Hasemi, Y. (January 01, 1986). Thermal Modeling Of Upward Wall Flame Spread. *Fire Safety Science, 1*, 87-96.
[54] Walters, R. N., Hackett, S. M., & Lyon, R. E. (September 01, 2000). Heats of combustion of high temperature polymers. *Fire and Materials, 24*, 5, 245-252.

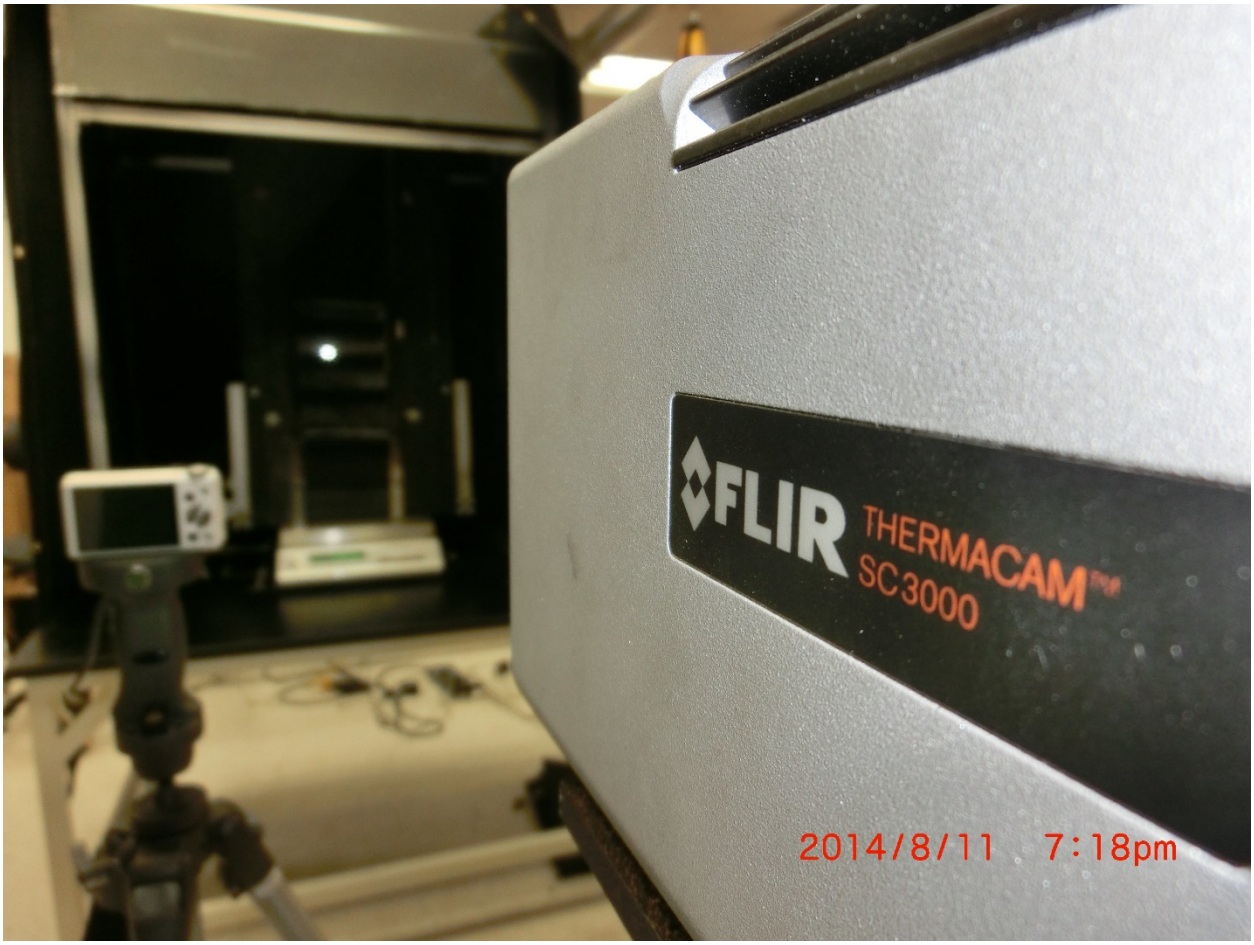
FLIR
THERMACAM
SC3000
2014/8/11 7:18pm